**Climate controls on the interseasonal and interannual variability of the surface mass balance of a tropical glacier (Zongo Glacier, Bolivia, 16°S): new insights from the application of a distributed energy balance model over 9 years**

**P. Autin**[1†], J. E. Sicart[1], **A. Rabatel**[1], **A.Soruco**[2]

[1] Univ. Grenoble Alpes, CNRS, IRD, Grenoble-INP, Institut des Géosciences de l'Environnement (IGE, UMR 5001), F-38000 Grenoble, France

[2] Facultad de Ciencias Geológicas, Universidad Mayo de San Andrés, La Paz, Bolivia

Corresponding author: Philémon Autin (philemon.autin@univ-grenoble-alpes.fr)

†Institut des Géosciences de l'Environnement, Bâtiment Glaciologie, 54, rue Molière, 38400 Saint Martin d'Hères – France

Key Points:

- Seasons over Zongo Glacier can be identified using the distribution of the cloud radiative forcings.
- The period between September and November is key in controlling the variability of the annual surface mass balance of Zongo Glacier.
- Distribution of the precipitation events in time is key in controlling the melt rate.

Abstract

The application of a distributed energy balance model over 9 years at an hourly time step to a 20×20 m grid cell over Glacier Zongo (Bolivia, 16°S) enabled assessment of the climate factors that control the interseasonal and interannual variability of its surface mass balance. The model was validated by comparing the measured and simulated discharge at the outlet, albedo at the AWS, surface types and annual mass balance both glacier wide and as a function of the altitudinal range. Analysis of the mean monthly energy fluxes highlighted the importance of the meteorological conditions during the period between September and November on the variability of the annual surface mass balance. Two sensitivity analyses are presented, one of the distribution of precipitation over time which maintains a physical coherence between the different meteorological variables and one of the impact of prolonged periods of intense cloud radiative forcing on the surface mass balance. The distribution of precipitation events over time and their associated amounts are the main drivers of the interannual variability of the surface mass balance via an albedo feedback effect. Additionally, prolonged periods of negative cloud radiative forcing, specifically over the month of November, have notable ability to reduce the melt rate.

**Plain Language Summary**

This study aimed at identifying the meteorological variables which control the seasonal and annual melt rates of a tropical glacier in Bolivia considering nine years of measurements at the hourly timescale. The analysis of the energy fluxes at the weather station has shown that the period between the austral winter and summer is the period during which most melt can be generated making it key in defining the annual melt rates. The analysis of the impact of measured meteorological variables on the melt rate has shown that it is the solar energy that controls most of it. The amount of solar energy available for melt is defined by the state of the glacier surface (snow, ice debris) of the glacier which controls the amount of reflected energy. In this context, the frequency of the snow fall events plays a key role in controlling the melt as frequent events imply a whiter glacier which is able to reflect most of the incoming solar energy. Similarly, because clouds can block large portions of solar energy, sustained cloud periods can play an important role on reducing the melt rate.

## 1 Introduction

In recent decades, both field observations and remote sensing have shown a trend of glacial retreat in tropical South America (e.g. Kaser, 1999; Soruco et al., 2009; Rabatel et al., 2013; Vincent et al., 2018; Dussaillant et al., 2019; Seehaus et al., 2020; Masiokas et al., 2020), linked by some authors to the global rise in air temperature (e.g. Bradley et al. 2009). However, only a few process-based studies, or short-period studies have been conducted to understand the complex climate-glacier relationships in the tropics (Wagnon et al., 1999; Sicart et al., 2005; Mölg et al., 2008, 2009; Litt et al., 2014; Maussion et al., 2015; Prinz et al., 2016).

Glacier surface mass-balance is controlled by the climate via energy and mass fluxes between the atmosphere and the glacier surface (Cuffey and Paterson, 2010). Specific climate conditions affect tropical including minor differences in seasonal air temperatures, marked precipitation seasonality, their very high elevations and the role of sublimation in the ablation processes (e.g., Sicart et al., 2011; Nicholson et al., 2013; Prinz et al., 2016). Understanding the relationship between mass and energy balances and identifying the key meteorological variables that control the glacier surface mass balance is crucial to better estimate past and future changes to glaciers and their consequences, for example, water availability whether it be for human consumption, irrigation or the production of hydroelectricity (e.g., Soruco et al. 2015).

In this context, distributed energy balance models are useful as they provide insight into the mechanisms that control glacier interseasonal and interannual surface mass-balance variability. Studies using energy balance models have already been carried out on Zongo Glacier, located in the outer tropical Andes of Bolivia. Wagnon et al. (1999) calculated the surface energy balance at the automatic weather station in the ablation area over one hydrological year (1997-1998). This was the first study of the annual surface energy balance over the glacier, and showed that the main driver of mass loss is the net all-wave radiation, which is primarily controlled by an albedo feedback effect. The authors

also pointed out that because the meteorological conditions favor sublimation during the austral winter (between May and August, also known as the dry season) the melt rate over this period is lower than over the rest of the year, a process originally identified by Kaser et al. (1990). Between 1999 and 2000, Sicart et al. (2011) applied the Distributed Energy Balance Model (DEBAM, Hock and Holmgren, 2005) over the whole glacier, with a focus on the interseasonal variability of the surface mass balance. This study highlighted the notable influence of processes that occur during the transition period between the dry (June to August) and wet season (January to March) on the annual surface mass balance.

Another modeling approach was applied by Lejeune et al. (2007) using the CROCUS-ISBA model forced by meteorological data measured at the automatic weather station located on the moraine of Zongo. These authors showed that the rapid melting of snow on the moraine mainly depends on incident solar radiation.

Different authors put forward different atmospheric/meteorological factors as being responsible for the interannual variability of the surface mass balance of tropical glaciers in the Andes. Some highlighted the importance of the onset of the wet season (Francou et al., 1995, Sicart et al., 2011). However, Ramallo's PhD thesis (2013) found poor correlations between the surface mass balance and the onset and end of the wet season primarily due to the difficulty in precisely identifying the latter as the wet season in the eastern Andes of Bolivia generally starts between mid-November and January. Other authors (e.g., Francou et al. 2001; Rabatel et al., 2013) focused on the importance of large scale climatic indices like ENSO that favor a higher surface mass-balance deficit due to reduced precipitation and increased air temperatures. Nevertheless, poor correlations have also been reported between the ENSO and the precipitation and/or the surface mass balance.

So far, no one has used a physically-based surface mass-balance model over several years to obtain deeper insights into the atmospheric/meteorological factors that control the interannual variability of Zongo glacier surface mass balance. In this study, we applied an updated version of DEBAM (Hock and Tijm-Reijmer, 2012) to a period of nine non-consecutive years. Although less complex than other physically-based models (e.g., CROCUS-ISBA), the advantage of DEBAM is that it requires a limited number of meteorological variables, meaning measurements are available for more hydrological years to calibrate and validate the model. Because the model uses seven different meteorological variables at an hourly time scale, it is perfectly suited to study the interannual variability of Zongo glacier mass balance and was already used by Sicart et al. (2011) to study the interseasonal variability of the surface mass balance.

The long dataset available for modeling offered a unique opportunity to investigate the climate factors that control interannual and interseasonal variabilities of the surface mass balance. Because the years are very contrasted, it is possible to perform various sensitivity analyses to test hypotheses on the meteorologi-

cal parameters that impact mass loss (as these can be applied over years that have a contrasted surface mass balance). In addition, this dataset allowed us to build scenarios by reshuffling days, thereby guaranteeing physical coherence between the measured meteorological variables and enabling us to create realistic scenarios.

In the following section we describe the location of Zongo glacier, its climate and climate-glacier interactions. In section 3, we describe the meteorological data we used as model inputs, the model and its calibration, and the methodology we used for two sensitivity analyses to estimate the impacts of: (i) the distribution of the precipitation events over time and (ii) sustained cloud cover, on the surface mass balance. In section 4, we present the model results to assess the energy fluxes over the glacier and their link to the surface mass balance. Finally, we present and discuss the results of the two sensitivity analyses.

## 2 **Study area and climate setting**

### 2.1 Zongo Glacier

Zongo glacier is located on the southern side of Huayna Potosi peak (16°15'S, 68°10'W, Cordillera Real, Bolivia). The Cordillera Real is on the eastern edge of the Altiplano in the western part of the Amazon basin. Zongo Glacier is a valley type glacier extending 2.8 km from about 6,000 m a.s.l. down to about 4,950 m a.s.l. and has a surface area of 1.7 km$^2$. In collaboration with the French research institute IRD, the Bolivian authorities started a meteorological, glaciological, and hydrological observation program on Zongo Glacier in 1991 (Francou et al., 1995; Ribstein et al., 1995). The location of the automatic weather stations on and around the glacier along with the ablation stakes have varied over time but measurements have continued uninterrupted since the beginning of the program, see Rabatel et al. (2013) for a detailed overview of the monitoring network and Figure A in the Appendix for the operating periods of the three automatic weather stations. Figure 1 shows the location of the glacier along with its monitoring network.

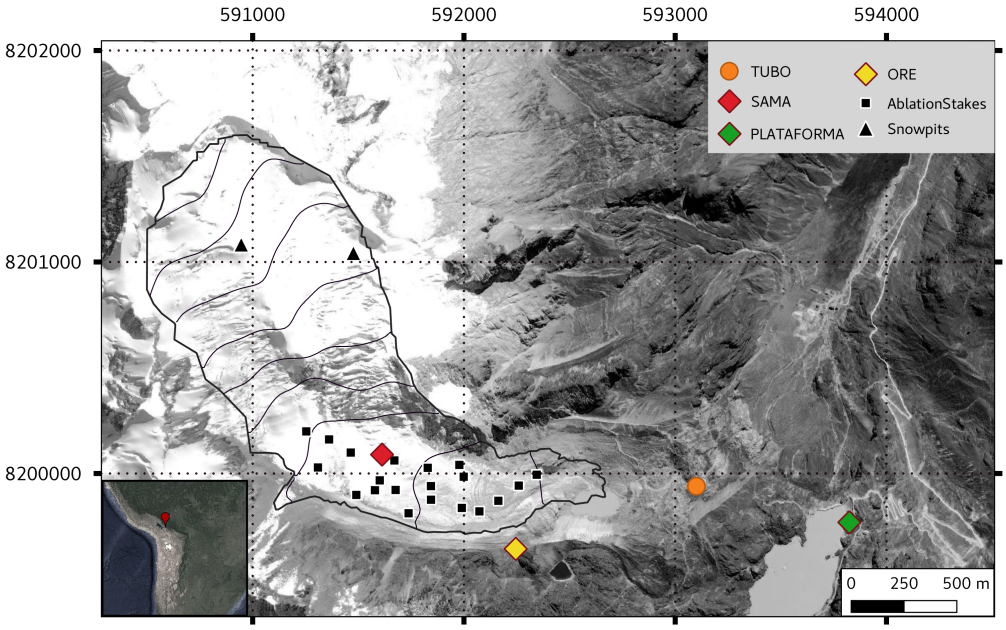


**Figure 1.** Location of Zongo Glacier and its monitoring network. SAMA is the on-glacier AWS, ORE is the AWS on the moraine and PLATAFORMA is the one at the pass. TUBO is a discharge gauging station. The bottom left rectangle shows the location of the glacier in South America.

2.2 Tropical climate and glaciological regime

As Zongo glacier is located in the outer tropics, its climate is characterized by marked seasonality of cloud cover and precipitation events that occur mostly during the austral summer, along with a pronounced dry season during the austral winter (Troll, 1941). The glaciological regime over this region was described by Kaser (2001): most accumulation occurs during the wet season (austral summer) whereas during the dry season (austral winter) predominant clear-sky conditions and dry air favor sublimation. This overall pattern has been well described from *in situ* monitoring, for instance by Kaser et al. (1990) over glaciers in the Cordillera Blanca or by Wagnon et al. (1999) over Zongo glacier. Conversely, Sicart et al. (2011) who ran DEBAM over Zongo glacier over the hydrological year 1999-2000 reported that the low melt rate during the dry season is linked to the large longwave emission deficit during this period.

Sicart et al. (2011) and Rabatel et al. (2012, 2013) identified three main seasons

on Zongo glacier based on observations of the interannual variability of Zongo's monthly surface mass balance in the ablation zone (Figure 2). Note that in order to account for the annual snow budget, the hydrological years for Zongo begin in September and end the following August.

As shown in Figure 2, from September to December, the ablation zone of Zongo glacier undergoes the highest surface mass losses with high melt rates (from -0.21 to -0.50 m w.e./month). This period is considered as the transition period between the dry and the wet seasons. It is also characterized by very high interannual variability of the surface mass balance (standard deviation of 0.29 m w.e./month on average for the three months). Ramallo's PhD thesis (2013) reported that about 20% of annual precipitation occurs during this period. Most cloud events over this period (80%, Sicart et al., 2016) are linked to northward propagating wind incursions to the east of the Cordillera (Surazos) that lead to deep convection events (Garreaud, 2000). Previous studies (e.g., Sicart et al., 2011) have shown that this period plays a key role in explaining the annual surface mass balance.

Between January and March, the surface mass balance in the ablation area is either slightly negative or positive. This period corresponds to the core of the wet season linked to the mature phase of the South American Monsoon System (SAMS). As the SAMS develops, the diabatic heating over the western Amazon leads to the formation of the anticyclonic system known as the Bolivian High in the upper troposphere (Lenters and Cook, 1997). Meanwhile, in the lower troposphere, the southward displacement of the South American Low Level Jet favors mean easterly winds on the northern arc of the Bolivian High, which in turn, allow the formation of strong heat-driven easterly winds on the eastern slopes of the Cordillera Real. These upslope winds transport moisture from the Amazon Basin to the tropical Andes. The solar heating of the surface leads to strong afternoon/early evening convection events in the Bolivian Andes and Altiplano (Garreaud et al., 2003). According to Sicart et al. (2016), nearly half the cloud events during this period can be linked to Surazo conditions. Throughout this period, there is little mass-loss as most of the observed melt comes from the snowfall events (70% of the annual amounts according to Ramallo's PhD thesis, 2013). Indeed, as shown by Sicart et al. (2011), throughout this season at the glacier snout, periods of snow melt during cloud events alternate with periods of ice melt during clear sky periods.

Finally, between June and August, the surface mass-balance in the ablation area becomes increasingly negative and both solar radiation and incoming longwave radiation are low. The large incoming longwave deficit leaves little energy available for melt (Sicart et al., 2005). In addition, the negative latent heat fluxes during this period favor strong sublimation (Wagnon et al., 1999). According to Ramallo's PhD thesis (2013), 10% of the annual precipitation occurs during this period and 87% of the cloud events can be linked to Surazo conditions (Sicart et al., 2016).

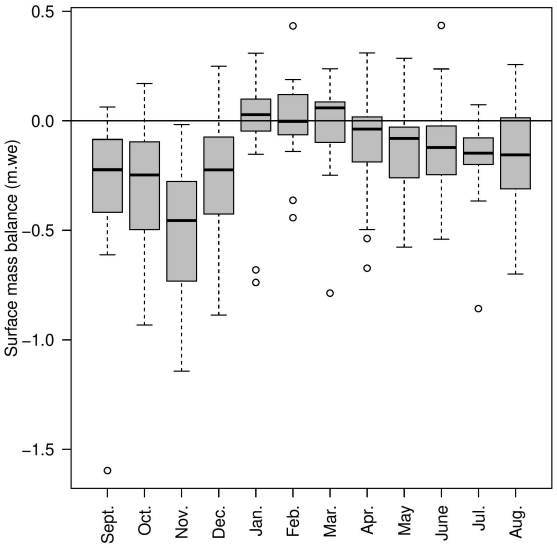


**Figure 2.** Box plot showing the monthly surface mass balance of the ablation area of Zongo Glacier (between 5,000 and 5,200 m a.s.l.) for the period 1991 to 2017.

Figure 3a, 3b show the annual cycles of incoming short and longwave radiation considering a 9-y daily average. The theoretical shortwave radiation at the top of the atmosphere increases steadily between September and November (Fig. 3a) and the incoming longwave radiation is highest during the core of the wet season (Fig. 3b). Sicart et al. (2010) showed that clouds increased the longwave radiation by up to 55% during the wet season and by about 20% on average. This effect contributes to the significant mass loss in the ablation area over the transition period (Fig. 2).

Figure 3a shows that incoming shortwave radiation is at its highest and the incoming longwave radiation (Fig. 3b) is at its lowest during the dry season; indicative of a majority of clear-sky days.

Similarly, during the transition period, the incoming shortwave radiation increases steadily, while incoming longwave radiation increases as the wet season approaches (when it is at its highest), highlighting increased frequency of cloud events, as reported by Sicart et al. (2010).

The present study of the incoming radiation fluxes and their link to the surface mass balance showed that both incoming short and long wave radiations are rather poorly correlated with the surface mass balance (R2 = 0.01 and 0.28 respectively at the annual scale based on nine years of data).

Figure 3c shows the interannual variability of the monthly mean temperatures at PLATAFORMA over a period of 14 years: the interannual variability of

the monthly average is low (the median values vary between 1.5 and 2.2°C). This low variability explains why the mean temperatures are poorly correlated with the annual glacier-wide surface mass balance at both monthly and seasonal scales. When considering the surface mass balance of the ablation zone, the best correlation obtained was R2 = 0.69 during the core wet season. Altogether, the best correlations with the glacier-wide surface mass balance were obtained at the annual scale but were nevertheless low ($R^2 = 0.18$).

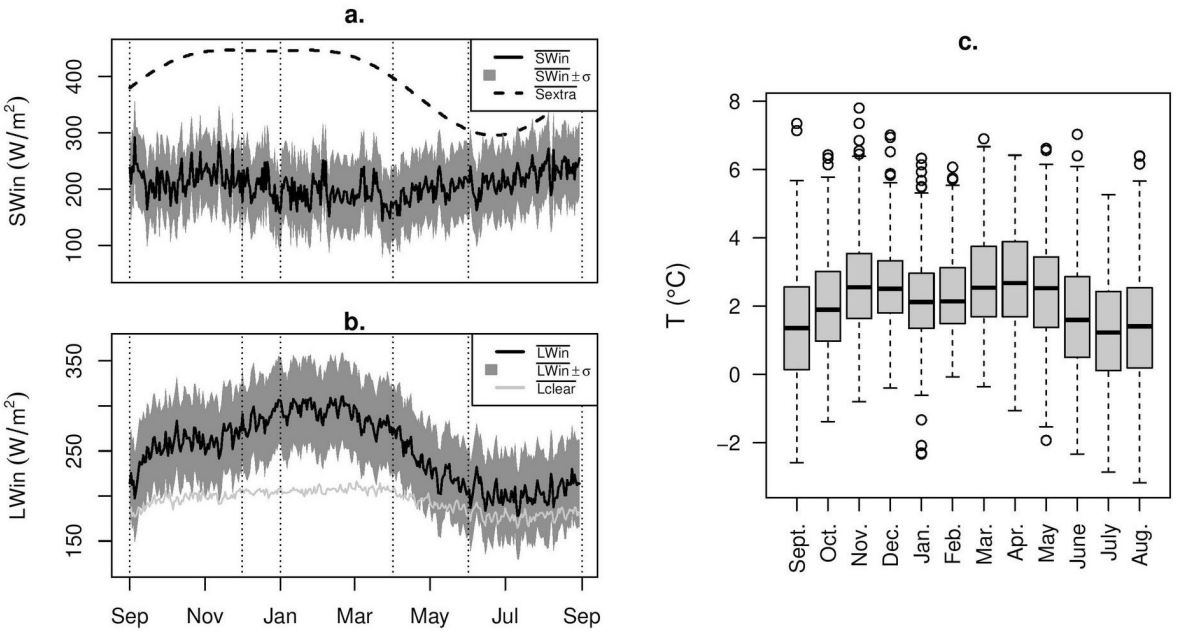


**Fi**

**3.** Annual cycle of (a) incoming shortwave radiation and theoretical radiation at the top of the atmosphere and (b) incoming longwave radiation. These two plots show daily incoming radiation averaged over the nine years studied. The boxplot (c) shows the interannual variability of the monthly mean temperature at the pass (PLATAFORMA weather station).

Seasons can also be defined by looking at the distribution of the cloud radiative properties and more specifically at cloud radiative forcing, i.e., the combined effect of the clouds on the incoming radiation: the increase in longwave emission and the reduction in incoming shortwave radiation, the latter being predominant. Based on the methodology presented in Sicart et al. (2016), 13 years of cloud radiative data were grouped and the monthly probability density functions were analyzed. The results of this analysis confirmed that three seasons can be distinguished: a transition period (when the melt rate increases) from September to November, a core wet season from January to March and a dry season from June to August.

Figure 4 shows the probability distribution functions of each season along with

that of the corresponding months. As can be seen in the figure, the groups based on cloud radiative properties are similar to those resulting from the analysis of the monthly surface mass balance interannual variability in the ablation zone. Between September and November (transition period, Fig. 4a), the bimodal distribution of the cloud radiative forcings suggests the presence of two different clouds: those with little impact on the radiation budget (cold high-altitude thin clouds), and clouds with a significant impact on the radiative budget evidenced by the peak around -120 W/m$^2$; i.e. thick warm clouds typical of convective events. During the core wet season (January – March, Fig. 4b) the cloud distribution is unimodal, and the peak is centered around -150 W/m$^2$, suggesting a majority of thick warm clouds. Finally, Figure 4c shows that the distribution is again unimodal during the dry season and is centered around -20 W/m$^2$ , making it possible to deduce that, during this period, the majority of the clouds are high altitude thin clouds with a negligible impact on the radiation budget.

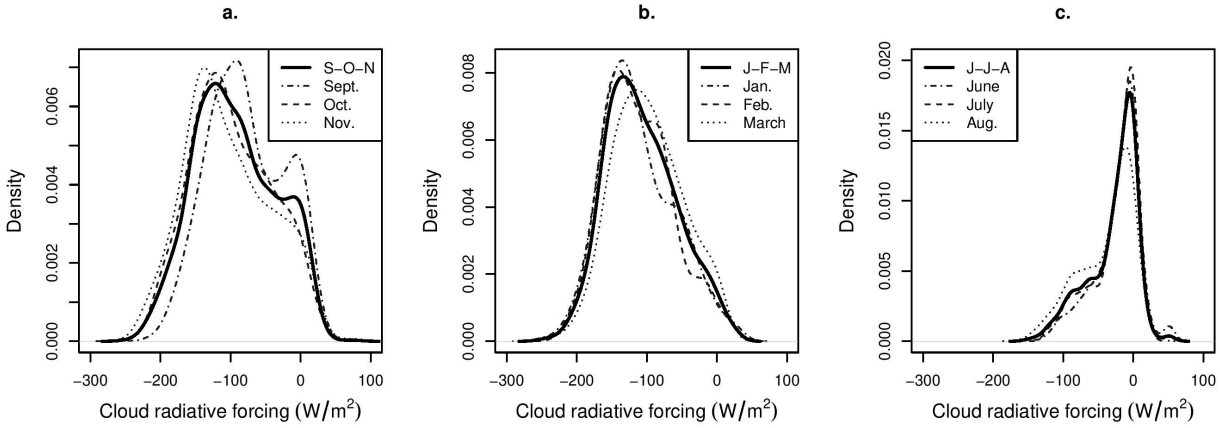


**Fi**

**4.** Probability distribution functions of cloud radiative forcing according to the season and their corresponding months (considering 13 years of data). Plot (a) shows the distribution of cloud radiative forcing in the transition period (September to November), plot (b) for the core wet season (January to March) and plot (c) for the dry season (June to August).

## 3 Data and methods

### 3.1 Input dataset

The model requires the following input variables: air temperature, precipitation, incoming shortwave and longwave radiation, outgoing longwave radiation, relative humidity, and wind speed. Due to the difficulty of maintaining fully operational automatic weather stations on the glacier, sufficient data were only available for nine non-consecutive years within an 18-year period from 1999 to

2017: 1999 to 2001, 2004 to 2006, 2008 to 2010, 2011 to 2013 and 2016-2017.

The data used as input variables for the model came from the SAMA automatic weather station located on the glacier surface at 5,050 m a.s.l. Table 1 lists the equipment used for the measurements. Appendix A details the gap-filling methodology used.

The precipitation data came from the ultrasonic gauge according to the methodology described in Sicart et al. (2002): the precipitation amounts were obtained by comparing the means of three consecutive measurements spread over one hour at 3-hour intervals, in order to identify changes in surface height of at least 1 cm. The amounts in water equivalent were then derived by applying a fresh snow density of 220 kg/m$^3$ for the transition period and the dry season and a density of 250 kg/m$^3$ for the wet season (due to slightly higher temperatures over the austral summer).

Because the modeled years were spread out over 18 years, a period during which the glacier lost 12% of its surface area and the altitude of the glacier front dropped 55 m, digital elevation models (DEMs) had to be reconstructed for each modeled year. The altitude of the glacier was interpolated (or extrapolated) linearly between two measured DEMs: one from 1997 based on aerial photographs (Soruco et al., 2009) and one from 2011 made from Pléiades satellite stereo-images (Cusicanqui et al., 2015). The glacier contours were based on differential GNSS measurements made each year during field campaigns.

Figure 5a illustrates the glacier retreat during the modeled period. Figure 5b shows the impact of accounting for a changing DEM compared to the impact of using the 1997 DEM on the simulated annual surface mass balance with respect to the reference measured annual surface mass balance (SMBref, Vincent et al., 2018). As can be seen in Figure 5b, the results obtained at the annual scale are much closer to the reference SMB values simply by accounting for the glacier retreat and changes in altitude. This significant improvement was due to the fact that accounting for the glacier retreat reduces the size of the ablation zone (by not including ice that is no longer there) thereby significantly reducing the melt. This was specifically true for years with a significant mass loss (e.g. 2004-2005).

The discharge data from the TUBO gauging station, a V-shaped weir with an automatic limnigraph, were used as validation data as these data are representative of the overall amount of melt water. Other data came from ablation stakes distributed all over the glacier surface that provide point surface mass balance values. Finally, photos taken during field campaigns were used to compare the modeled and observed glacier surface state (e.g. snow or ice).

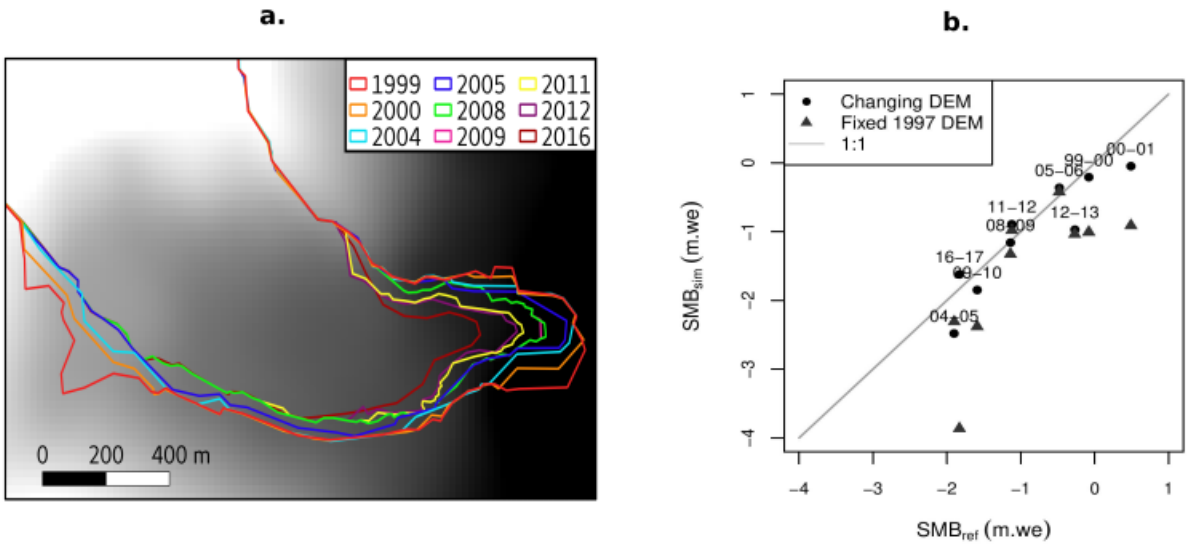


**5.** (a) Changes in the position of Zongo glacier front between the first and the last modeled year (the glacier lost 12% of its surface area and the altitude at the glacier front dropped by 55 m). (b) Impact on the surface mass balance simulations of using annually updated DEMs and glacier outlines. The straight line represents the measured surface mass balance (1:1), the dots are the simulation results considering an annual DEM and glacier contour and the triangles represent the simulated SMB considering simulations with a 1997 DEM and glacier contour. $SMB_{sim}$ refers to DEBAM simulated values. $SMB_{ref}$ refers to measured values.

**Table 1.** List of the equipment at SAMA along with the sensor heights and precision according to the manufacturer

| **Variable** | **Sensor** | **Sensor heigh** |
|---|---|---|
| Temperature (°C) | CS2115 (since 23/02/2011) | 1.00 m |
| | Vaisala HMP45C (up to 23/02/2011) | 1.57 m |
| Relative humidity (%) | CS2115 (since 23/02/2011) | 1.00 m |
| | Vaisala HMP45C (up to 23/02/2011) | 1.57 m |
| Wind speed (m/s) | Gill Solent (since 23/02/2011) | 1.74 m |
| | Young 05103 (up to 23/02/2011) | 2.50 m |
| Incoming and outgoing shortwave radiation ($W/m^2$) | Kipp&Zonen CM3 0,305< <2,8 m | 1.00 m |
| Incoming and outgoing longwave radiation ($W/m^2$) | Kipp&Zonen CG3 5< <50 m | 1.00 m |
| Snow height, ultrasonic measurements (m) | Campbell, SR50AT | 1.15 m |

3.2 Model description

The distributed energy model used in this study was DEBAM (Hock and Tijm-Reijmer, 2012) which solves the following energy balance equation (equation

1):

$$Q_M = G(1- \ ) + LW_{net} + H + LE + Q_G + R \quad (1)$$

where **QM** is the energy available for melt, **G** is the global shortwave radiation, the albedo, **LWnet** the net longwave radiation balance, **H** and **LE** are the sensible and latent heat turbulent fluxes, respectively, **QG** is the ground heat flux and **R** the sensible heat supplied by rain (negligible over Zongo as shown by Sicart et al., 2011). The model convention is such that energy fluxes directed towards the surface are positive and those away from the surface are negative.

The model was run at the hourly time scale over a distributed 20×20 m grid. First, the melt rate was calculated at the automatic weather station. The energy fluxes were then extrapolated across the glacier. Finally, three linear reservoirs representing snow, firn and ice were used to simulate the melting discharge using storage constants of 350, 30 and 16 h respectively according to Sicart et al. (2011).

All the parameters used in the present study were calibrated considering observations with physically coherent values. We chose not to use automatic calibration to avoid error compensation.

**Incoming radiation fluxes**

Global radiation was split into direct and diffuse components using a calibrated empirical relationship between the ratio of global radiation at the top of the atmosphere and the potential diffuse radiation: considering a clear sky attenuation of 13% at the daily time scale (according to Sicart et al., 2011). The diffuse radiation component was considered to be spatially variable and extrapolated according to topographic shading based on the sun's path and the effective horizon and sky view factor of the grid cell (Hock, 1998; Sicart et al., 2011). The direct component of the incoming shortwave radiation was extrapolated according to the slope and orientation of the grid cells (Sicart et al., 2011). The incoming longwave radiation was measured and assumed to be spatially constant over the glacier, a reasonable hypothesis given the small glacier surface area (1.7 $km^2$).

**Parameterization of the albedo**

Because DEBAM was originally developed to model glaciers in the Northern Hemisphere, a key adaptation to the way the albedo is calculated was implemented in the model by Sicart (2002). It consists of a modified version of Oerlemans and Knap (1998)'s albedo parameterization that accounts for the rapid alternation of accumulation and melt in the wet season as well as the impact of ice on the albedo over shallow snow depths:

In the absence of precipitation, the snow albedo decreases as follows:

$$_{snow} = \ _{firn} + (\ _{fresh\text{-}snow} - \ _{firn})e^{-nj\ /n*} \quad (2)$$

$$= \ _{snow} + (\ _{ice} - \ _{snow}\ )(1 + e_s\ /e_s^{\ *})^{-3} \quad (3)$$

where **n*** is the time constant of decrease in albedo (10 days), **es** the snow depth and **es*** the critical snow height below which the ice starts to influence the modeled albedo, considered here to be 6 mm w.e. according to Sicart (2002).

During precipitation events, the albedo increases proportionally to precipitation intensity (**Pr**):

$$= c_p Pr \quad (4)$$

where **cp** = 0.02 h/mm w.e. based on Sicart (2002). Based on previous studies (e.g. Sicart et al., 2002) the albedo values retained were 0.85 for fresh snow, 0.6 for firn, and 0.3 for ice.

**Glacier surface temperature**

Surface temperature was estimated from measured outgoing longwave radiation. It was then extrapolated across the glacier using a constant temperature lapse rate of -0.55 K/100 m according to Sicart et al. (2011).

**Estimation of turbulent energy fluxes**

The sensible and latent turbulent heat fluxes were calculated according to equations 5 and 6 considering atmospheric stability based on the Monin-Obukhov similarity theory (equations 7 and 8, Hock and Holmgren, 2005).

$$H = \rho c_p \frac{k^2}{\left[\ln\left(\frac{z}{z_{0W}}\right) - \Psi_M\left(\frac{z}{L}\right)\right]\left[\ln\left(\frac{z}{z_{0T}}\right) - \Psi_H\left(\frac{z}{L}\right)\right]} u\,(T_z - T_0) \quad (5)$$

$$LE = L_v \frac{0.623\rho_0}{P_0} \frac{k^2}{\left[\ln\left(\frac{z}{z_{0W}}\right) - \Psi_M\left(\frac{z}{L}\right)\right]\left[\ln\left(\frac{z}{z_{0e}}\right) - \Psi_H\left(\frac{z}{L}\right)\right]} u\,(e_z - e_0) \quad (6)$$

where $\mathbf{c_p}$ is the specific heat capacity of air at constant pressure (1005 J/kg/K), **k** is the Von Karman constant (0.41), $\mathbf{P_0}$ the standard atmospheric pressure (1013.25 hPa), $_{\mathbf{0}}$ is the air density at $\mathbf{P_0}$ (1.29 kg/m$^3$), $\mathbf{T_0}$ the surface temperature, $\mathbf{e_0}$ the surface water vapor pressure. $\mathbf{z_{0w}}$, $\mathbf{z_{0T}}$ and $\mathbf{z_{oe}}$ are the roughness lengths of wind and temperature and water pressure respectively, **z** is the instrument height. The roughness height of wind over ice was estimated over two field campaigns carried out on Zongo in July-August 2007 and June 2011 when eddy-covariance measurements were underway: the retained roughness height of the wind over ice was 26 mm, in agreement with the values found in Sicart et al. (2014). The ratio of the wind (and temperature) roughness height over ice and over snow was considered to be constant and set at 10. $\mathbf{L_v}$ is the latent heat of evaporation (2.514×10  J/kg). **M** and **L** are the stability functions that were assumed to be constant across the glacier (based on Beljaars and Holtslag, 1991 for the stable cases and based on the Businger-Dyer expressions from Paulson (1970) for the less frequent unstable cases). Equations 7 and 8 show how the stability functions are calculated in stable cases. **L** the Monin Obukhov length, which is defined according to equation 9. This formulation of the latent heat flux implies that when it is positive, if the surface temperature is 0 °C, condensation occurs, whereas if the surface is at subfreezing temperatures, it re-sublimates. Similarly, if the latent heat flux is negative then sublimation is

expected to occur regardless of the surface temperature (Hock and Holmgren, 2005).

$$-\Psi_M = \frac{\mathrm{az}}{L} + b\left(\frac{z}{L} - \frac{c}{d}\right) e^{(-d\frac{z}{L})} + \frac{\mathrm{bc}}{d} \quad (7)$$

$$-\Psi_H = \left(1 + \frac{2\mathrm{az}}{3L}\right)^{1.5} + b\left(\frac{z}{L} - \frac{c}{d}\right) e^{(-d\frac{z}{L})} + \frac{\mathrm{bc}}{d} - 1 \quad (8)$$

$$L = \frac{\rho c_p u_{\mathrm{star}}^3 T_z}{\mathrm{kgH}} \quad (9)$$

where $\mathbf{u_{star}}$ is the friction velocity calculated according to equation 10 and $\mathbf{T_z}$ the temperature at instrument height (in Kelvin). In order to calculate **L,** H, LE and $u_{star}$ must be known, thus, it is defined by iteration for each time step following the procedure described by Munro (1990). To avoid too much reduction in turbulent energy, in the case of very high stability, the minimum value of Obukhov's length (**L**) was set at 0.3.

$$u_{\mathrm{star}} = \frac{k u_z}{\ln\left(\frac{z}{z_{0W}}\right) - \Psi_M} \quad (10)$$

**Other model parameterization of interest**

Air temperature was extrapolated using a constant lapse rate of -0.55 K/100 m. A precipitation gradient of +10% /100 m was applied up to 5,400 m a.s.l. At the beginning of each year, the model was supplied with a map of the limit of the firn estimated based on in-situ terrestrial photographs or LANDSAT images and with a map of fresh snow cover (based on field photographs).

This model has been used and validated in many studies in the Northern Hemisphere, e.g. by Hock and Holmgren (2005), Reijmer and Hock (2008), Østby et al. (2017) and on Glacier Zongo by Sicart et al. (2002, 2011).

3.3. Model validation

Because we chose to use a constant set of parameters for the nine years to guarantee robust calibration, the calibration process involved a trade-off between very precise modeling of specific years (e.g. years with high precipitation) and obtaining a globally efficient parameter set. Special emphasis was placed on reproducing the transition periods as accurately as possible as they play an important role in the interannual variability of the surface mass balance (Sicart et al., 2011).

To validate model performances, we chose to focus on the following observations: the measured albedo at SAMA (when available), the measured melting discharge, observations from terrestrial photographs to compare observed and modeled glacier surface states, the measured glacier-wide surface mass balance, and the surface mass balance as a function of altitude.

Figure 6 illustrates the results for the year 1999-2000. This year was chosen because it has already been studied in depth by Sicart et al. (2011). Figure 6a shows the observed and simulated daily mean albedo. Variations in albedo are

well represented but the amplitude is sometimes off, suggesting that precipitation events are well represented, but not always their intensity. This is due to both the marked uncertainties in measurements of precipitation at the hourly timescale (Sicart at al., 2002) and to the fact that the same set of parameters is used for the whole year although it is known that the snow melts faster in the wet season than in the dry season (Sicart et al., 2011) leading to different albedo decay rates that are not accounted for by the model.

This is a non-negligible source of error because erroneous albedo parameterization leads to errors on the simulated glacier surface that have a significant impact on the melt rate, as solar irradiance is often the main source of fusion (Sicart et al., 2005) and is controlled via an albedo feedback effect (and hence the glacier surface). In addition, errors on the simulated surface lead to erroneous turbulent flux simulations via the retained roughness height of the wind and the temperature in the model.

Figure 6b shows the modeled and observed discharge. The modeled discharge is slightly overestimated between January and May but is well simulated for the rest of the year.

According to Sicart et al. (2011) a variety of error sources can explain the differences between measured and simulated results. In the model, the surface temperature is calculated using the measured outgoing longwave radiation at the weather station and extrapolated by applying a constant lapse rate, as a result, the model is not able to capture the intense night cooling of the surface in the firn area, which in turn, delays the diurnal melting period of the surface, leading to potential overestimation of the melt rate. Furthermore, erroneous surface temperatures affect the simulated turbulent fluxes and in turn, affect the surface temperature, leading to rapid uncertainty propagation. This process is particularly important in the dry season when nighttime cooling of the surface in the accumulation area is at its highest.

Finally, Figure 6c shows the surface mass-balance as a function of altitude and gives an idea of the overall model performance at the annual scale. For this particular year, the model performs well as the measured and modeled equilibrium lines are very similar (difference of less than 40 m of altitude).

Figure B in the appendix shows the measured and simulated surface mass balance as a function of altitude for all nine years covered in this study. Overall, the simulated equilibrium line is in good agreement with the measurements. One of the main drawbacks of considering a single calibration for all the modeled years is that the model is not equally accurate for each of the years modeled: in some years, melt in the ablation zone is underestimated (e.g. 2005-2006) whereas in others, it is overestimated (e.g. 2004-2005). Considering the 9-y average, the overall mass loss is overestimated by 0.18 m w.e. when the average surface mass balance is -0.88 m w.e. The simulation errors for years with a significant mass loss tend to be higher than for years with a limited mass loss.

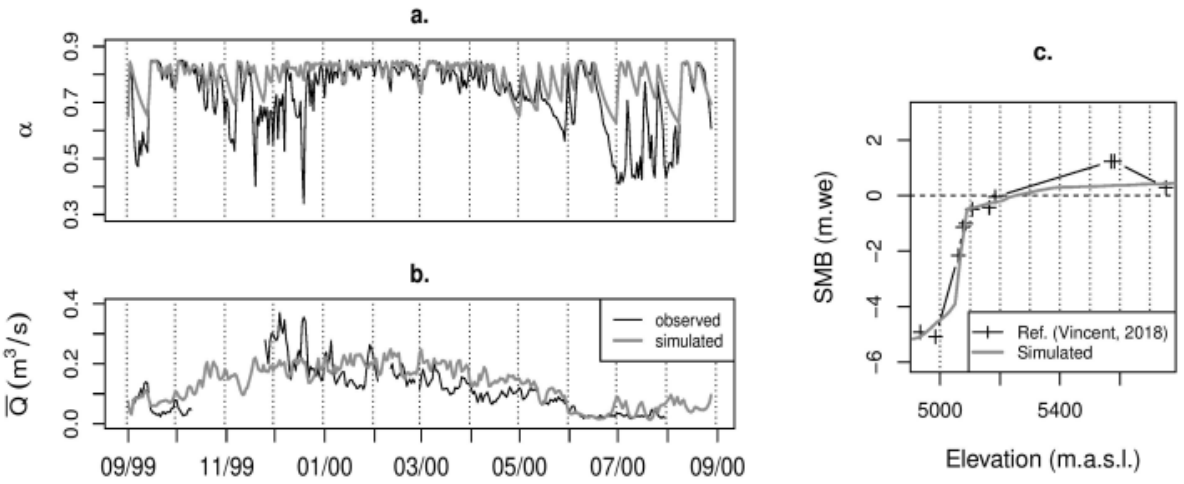


**Figu**

**6.** Validation of the model results for the year 1999-2000. Plot (a) shows the daily mean albedo, plot (b) mean discharge and plot (c) the specific surface mass balance according to altitude.

3.4 Methodology used for the generation of the scenarios for precipitation sensitivity analysis

The aim of this study was to analyze the impact of the distribution of the precipitation events over time during the transition season on the surface mass balance. To guarantee physical coherence between the different meteorological variables in the scenarios, not only the precipitation variables, but all the measured variables on the corresponding day, were shuffled. Hence, if precipitation events on day X (a day with no precipitation), were required to build a scenario, a day with precipitation (Y) was selected and days X and Y were swapped along with all the measured variables of interest.

Initially three contrasted years were selected based on the average plus or minus half of the standard deviation of the annual surface mass balance (-0.88 ± 0.42 m w.e.). of the nine years modeled. 1999-2000 (SMB = -0.08 m w.e.) was selected as the year with limited melt, 2008-2009 (SMB = -1.14 m w.e.) was selected as a year in which the SMB was close to the 9-year average. 2004-2005 was selected as the year with significant mass loss, as it had the highest recorded mass loss of the nine years studied (SMB = -1.90 m w.e.).

For these years, the following three scenarios were generated:

- S1: even redistribution of the days with precipitation events greater than or equal to 2 mm/d. The threshold of 2 mm/d was chosen because it corresponds to a precipitation amount that allows the formation of at least 1 cm of snow, which in turn, enables significant changes in albedo values and hence has an impact on the melt rate.
- S2: even redistribution of the days on which the precipitation events ex-

ceeded 9 mm/d (that enabled investigation of the impact of the threshold value).

- S3: all the precipitation events exceeding 2 mm/d that occurred in a given month were stacked at the beginning of the month.

Moving days around to generate the scenarios impacted net incoming radiation at the glacier surface via cloud radiative forcing as moving precipitation events also involved moving clouds. But, as melt was generally limited during precipitation events, the cloud radiative forcing induced by moving the clouds was of little importance.

3.5. Methodology used to build scenarios for cloud sensitivity analysis

To assess the impact of the cloud radiative properties on the surface mass balance during the transition period, a different methodology had to be used to generate the scenarios since moving days that met certain cloud radiative properties involved moving precipitation events. Thus, the impact of the clouds on the surface mass balance was mitigated by the altered precipitation patterns.

Consequently, the scenarios were generated by recalculating the incoming radiation fluxes based on specific cloud radiative properties without changing the other measured variables used as model inputs. To achieve this, the bulk cloud shortwave transmissivity ($Tn$) and cloud longwave emission factors ($F$) were derived from the long term (9-yr) monthly 66th percentile of the absolute value of the cloud radiative forcing. Tn represents solar attenuation due to the presence of clouds and F represents the increase in longwave emission linked to the presence of cloud (Sicart et al., 2010, 2016).

We chose to use the 66th percentile of the 9 years to guarantee a thick cloud cover which is realistic as the cloud radiative forcing measured on 34% of the days was actually above this value. Table 2 lists the cloud radiative properties for each month. These values are typical of thick warm clouds: regardless of the month considered, the clouds reduce the incoming shortwave radiation by at least 47% and increase the incoming longwave radiation by at least 23% (N.B. Sicart et al., 2016 considered that clouds have a significant impact on the radiative budget when F  1.15).

To obtain incoming radiation fluxes corresponding to these cloud radiative properties, the incoming longwave radiation (**LWin**) was calculated according to equation 11:

$$LW_{in}{}^{cloud} = (F^{cloud}/F^{meas}).LW_{in}{}^{meas} \quad (11)$$

Similarly, the incoming shortwave radiation ($\mathbf{SW_{in}}$) was calculated using the ratio of the selected bulk shortwave transmissivity ($\mathbf{Tn^{cloud}}$) over the measured bulk shortwave transmissivity ($\mathbf{Tn^{meas}}$) as shown in equation 12.

$$SW_{in}{}^{cloud} = (Tn^{cloud}/Tn^{meas}).SW_{in}{}^{meas} \quad (12)$$

Scenarios were generated for all nine years studied: one for each month of the transition period with sustained cloud cover lasting throughout the month:

- Sce_S: cloud cover throughout September
- Sce_O: cloud cover throughout October
- Sce_N: cloud cover throughout November

Although changing the incoming radiation fluxes values led to a loss of physical coherence between the different meteorological variables (temperature, relative humidity, and wind speed), the loss was considered acceptable as the main impact is on the turbulent fluxes which, according to Sicart et al. (2011), remain low during the transition period.

**Table 2.** Summary of the $66^{\text{th}}$ percentile value of the cloud radiative forcings per month/season and the corresponding F and Tn values retained for the scenario. As can be seen in table, the cloud radiative forcing values retained are consistent with the distribution of the cloud radiative forcing presented in Figure 4a.

| Month | $66^{\text{th}}$ percentile value of CF ($W/m^2$) | F | Tn |
|---|---|---|---|
| September | -109 | 1.42 | 0.47 |
| October | -128 | 1.30 | 0.51 |
| November | -136 | 1.23 | 0.53 |

## 4. Results and discussion

### 4.1. Analysis of the interannual variability of the simulated energy fluxes

Table 3 shows the modeled annual surface mass balance, melt and precipitation along with the extent they differ from the 9-year average. The years in italic are years in which the mass loss can be considered limited (SMB > SMB + /2): 1999-2000, 2000-2001 and 2005-2006. The years in bold are the three years in which the mass loss is significant (SMB < SMB + /2): 2004-2005, 2009-2010 and 2016-2017. As can be seen, years with limited loss are years when the precipitation amounts were above average ($P > \underline{P} + \frac{\sigma}{2}$), similarly, years with a significant mass loss were years with a precipitation deficit ($P < \underline{P} - \frac{\sigma}{2}$).

**Table 3.** Simulated annual surface mass balance and melt and annual precipitation in the nine years, along with the differences from their respective mean values. The three years in italics are years in which the mass loss is significantly less than the average (SMB > SMB + /2). The three years in bold are those in which the mass loss is significant (SMB < SMB – /2)

| Years | Annual scale values | | | Difference from mean values $(X - \overline{X})$ | | |
|---|---|---|---|---|---|---|
| | SMB (m w.e.) | Melt (mm w.e.) | Precipitation (mm) | SMB (m w.e.) | Melt (mm w.e.) | Precipitation (mm) |
| *1999-2000* | *-0.21* | *1925* | *1740* | *0.85* | *-642* | *132* |
| *2000-2001* | *-0.04* | *2033* | *1981* | *1.02* | *-534* | *373* |
| **2004-2005** | **-2.47** | **3493** | **1348** | **-1.41** | **926** | **-260** |
| *2005-2006* | *-0.36* | *2252* | *1913* | *0.70* | *-315* | *305* |
| -2009 | | | | | | |
| **2009-2010** | **-1.84** | **2998** | **1473** | **-0.79** | **432** | **-136** |
| -2012 | | | | | | |
| -2013 | | | | | | |
| **2016-2017** | **-1.62** | **2960** | **1317** | **-0.56** | **393** | **-291** |
| | | | | NA | NA | NA |

The monthly cumulated energy fluxes at the automatic weather station (SAMA) are presented in Figure 7. The fluxes at the AWS are presented rather than the glacier-wide fluxes in order to limit simulation errors due to the strong hypotheses applied to the spatial extrapolation (arbitrary temperature and precipitation gradients).

When considering the 9-year average annual energy cycle (Fig. 7a), the energy balance is at its lowest during the dry season (June to August). During this period, in contrast to the rest of the year, the net longwave radiation deficit is at its highest due to the combined influence of intense surface night cooling and absence of clouds that emit longwave radiation (Sicart et al., 2011). Conversely, during the transition period, the increase in surface temperatures combined with the increased frequency of cloud events and the increase in incoming solar radiation, mean large amounts of energy are available for melt.

Figures 7b and 7c show the monthly energy fluxes for two contrasted years: 2016-2017 (SMB= -1.62 m w.e.) and 1999-2000 (SMB = -0.21 m w.e.). Figure 7b shows that much more energy is available for melt in the year with a significant mass loss than the long-term average because of a significantly higher shortwave

energy budget (the longwave one being similar to that of the long term average).

When considering the year with a limited mass loss (Fig. 7c), one can see that although some energy was available for melt during the wet season, the sum of the energy fluxes was mostly negative for the rest of the year resulting in surface cooling rather than melting. Once again, the differences between this year and the long-term average are mainly explained by a lower net shortwave radiation budget and hence a higher glacier wide albedo.

Considering all three plots (Fig. 7a to c), it is clear that the transition period controlled most of the annual surface mass balance as, both on average and for the year with significant mass loss, the transition period is when most energy is available for melt. When the sum of the energy fluxes is negative or close to zero during this period, the annual mass loss is significantly lower than average (Fig 7c).

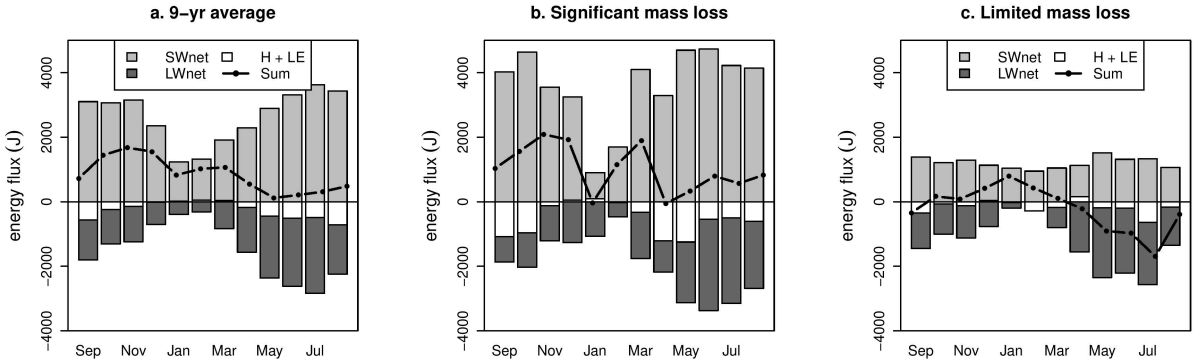


**Fi**

**7.** Plot (a) shows the mean monthly energy fluxes for the 9 years concerned. Plot (b) shows the mean monthly energy fluxes for a year with a highly negative surface mass balance (2016-2017, -1.62 m w.e.) and plot (c) for a year with limited mass loss (1999-2000, -0.21 m w.e.). The cumulated energy fluxes shown are the simulated fluxes at the automatic weather station (SAMA). Note, a positive sum implies that energy is available for melt, whereas a negative one implies surface cooling via the ground heat flux.

To better understand the interannual variability of the surface mass balance, three years with limited melt: 1999-2000, 2000-2001 and 2005-2006 were compared to three years with a significant mass loss: 2004-2005, 2009-2010 and 2016-2017 (see Table 3 for the surface mass balance values).

This study (illustrated by the comparison of the year 1999-2000 and the year 2016-2017 in Figure 8) showed that during the transition period, years with limited mass loss systematically had a higher glacier-wide albedo (Fig. 8a). This trend was sometimes inverted between March and May. At the annual scale, the mean annual albedo of the three years with limited melt was 13% higher than the mean annual albedo of years with significant melt. During the

transition period, the mean annual albedo was 11% higher, while during the dry season it was 30% higher. However, during the core wet season, it was only 1% higher, the small difference being due to the frequent precipitation events during this period regardless of the year considered.

In addition, years with a significant mass loss tended to be less cloudy than years with a limited mass loss (Fig. 8b). This is underlined by the mean monthly cloud index developed by Sicart et al. (2016): the higher the index, the greater the ability of the clouds to block incoming solar radiation. At the annual scale, the mean CI of the three years with limited mass loss was 15% higher than the mean CI for years with significant mass loss and at least 6% higher regardless of the season considered.

Although the differences in mean glacier wide albedo and cloud index between years with low and high melt rates were of the same order of magnitude, it is the albedo that controls the largest portion of the net energy budget. This is because, in terms of energy amounts, incoming solar radiation is significantly more powerful than cloud radiative forcing. Hence, via a feedback effect, a higher albedo reduces the total melt energy more than the radiation deficit created by the cloud radiative forcing.

This analysis showed that the transition period is most important in terms of controlling the interannual variability of the surface mass balance mainly because it is the period where the solar radiation approaches its highest value with still only sporadic cloud events, meaning it has the highest net incoming radiation. This coupled with the fact that during the transition period, the temperature at the glacier surface is close to 0°C, the conductive heat flux in the ice and snow is negligible, when the sum of the radiation fluxes on the glacier's surface is positive, the excess energy is consequently converted into melt.

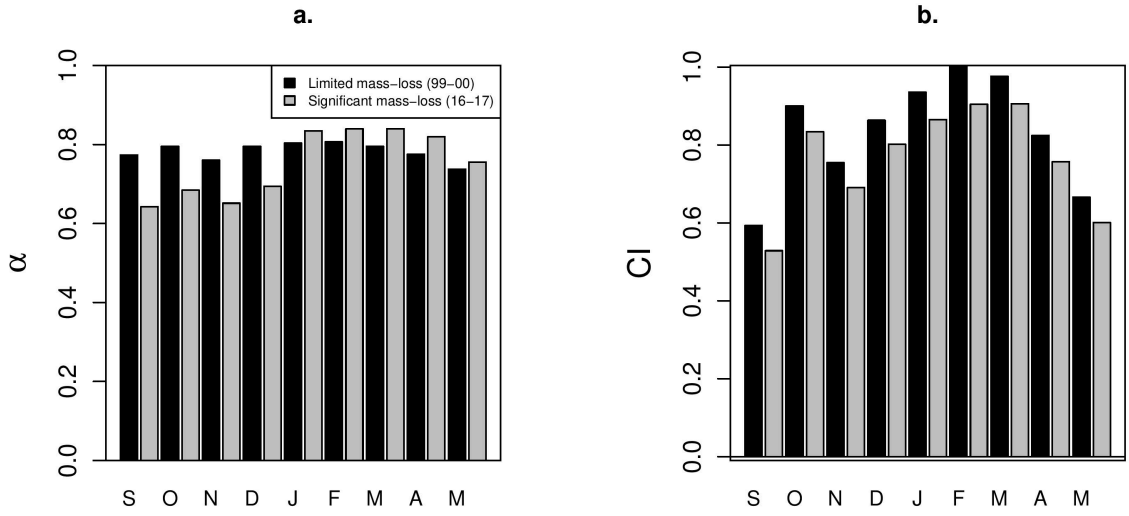


**Fi**

**8.** Comparison of (a) monthly mean glacier-wide albedo, (b) mean monthly cloud index for two contrasted years. The year 1999-2000 is in black (limited mass loss: SMB= -0.21 m w.e.) and the year 2016-2017 is in gray (significant mass loss: SMB = -1.62 m w.e.).

4.2. Sensitivity study of the distribution of precipitation events over time

4.2.1 Application of the three scenarios to three contrasted years

Precipitation amounts and frequencies display marked interannual variability. Accordingly, the interannual variability of the surface mass balance is primarily due to the albedo feedback effect. Analysis of two precipitation characteristics (amounts and number of events above 2 mm/d) at the annual scale over 18 years revealed close links with the surface mass-balance ($R^2$= 0.44 and 0.52, respectively). Hence, a sensitivity analysis of the temporal distribution of the precipitation was deemed of interest.

Figure 9 shows the main impacts of the scenarios on the physical processes affecting the glacier in the 2008-2009 transition period. This year was chosen to illustrate the results as similar behaviors were observed in the three contrasted years to which the scenarios were applied (1999-2000: limited mass loss, 2004-2005: significant mass loss and 2008-2009: average mass loss). All the plots in figure 9 show the differences between the results obtained with the scenarios compared to the results obtained with the reference run (i.e., the run with measurements used as model inputs). Thus, a positive difference implies a higher value obtained with the scenario than with the reference simulation.

Figure 9a shows that evenly redistributing the precipitation events (S1 and S2)

maintained a thicker layer of fresh snow covering the glacier throughout the season, which can be expressed by a generally higher albedo (Fig. 9b) and hence a lower net shortwave radiation balance (Fig. 9c), which in turn, resulted in a lower melt rate (Fig. 9d). When considering the average reduction in melt of the three years considered over the transition period, scenarios S1 and S2 reduced the melt rate by 7% and 2%, respectively, whilst scenario S3 increased the melt rate by 12%. Note that because scenario S1 involved moving more precipitation events than scenario S2, it reduced the melt rate more than the latter (as it maintained a thicker glacier fresh snow cover).

On the other hand, scenario S3 grouping all the precipitation events at the beginning of the month yielded a much thicker snow cover at the beginning of the month (except in September 2008, due to a small amount of measured precipitation: 29 mm w.e.). However, due to a lack of precipitation for the rest of the month, this snow cover disappeared, resulting in a lower albedo than in the reference run, and thus, over the whole period, to higher cumulated melt.

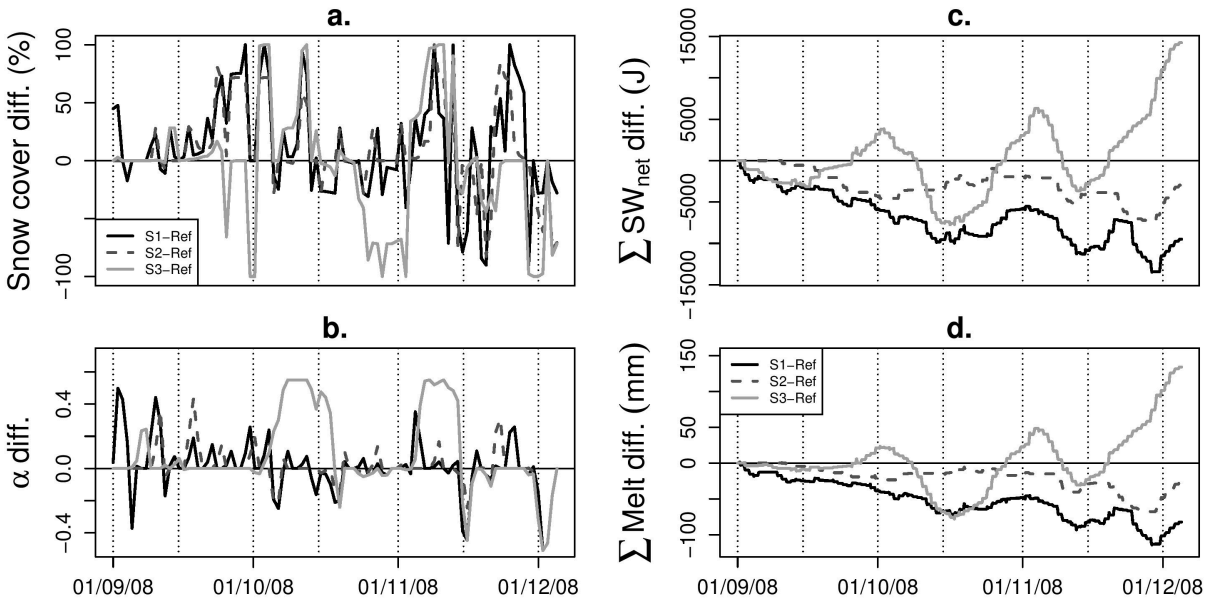


**Fi**

**9.** Glacier-wide impact of the scenarios on (a) the fresh snow cover, (b) the albedo, (c) net shortwave radiation and (d) melt compared to the reference run between September and November 2008.The results presented here shows the values obtained with the scenarios minus the reference run (i.e., the run with measurements used as model inputs) hence, a positive difference in the plots means a higher value was obtained with the scenario than with the reference run.

The impact of each scenario on the surface mass balance over the transition period in the three years considered is shown in Figure C in the appendix.

Although scenario S1 systematically resulted in a smaller mass loss than the reference run, the effects of scenarios S2 and S3 were contrasted, with a significant difference for the 2004-2005 transition period: scenario S3 limited the melt most and scenario S2 increased mass loss.

In 2004-2005, scenario S1 did not reduce the mass loss as it did in the other two years because the precipitation events were already rather well distributed over time (data not shown). Consequently, in contrast to the other years, the impact of scenario S1 was attenuated. The monthly scale (table C in the appendix) shows that the melt rate was lower for September and October due to increased precipitation events. On the other hand, in November, scenario S1 resulted in six fewer precipitation events, and, combined with the fact that November is the month with the highest potential solar irradiance, there was an overall decrease in the glacier-wide albedo that significantly increased the melt rate. As a result, all the reduction in melt rate obtained between September and October was offset by the increased melt rate in the second half of November.

In contrast, scenario S3 limited the mass loss more than the other scenarios and more than the reference run, as it allowed the formation of a thick snow-pack over the glacier. This snow-pack remained throughout the rest of the month thanks to numerous precipitation events of less than 2 mm/d (hence left untouched in the scenario).

Additionally, in this year, seasonal precipitation was lower than the 9-year average: 294 mm versus 334 mm, partly explaining the significant mass loss. Table 4 lists the seasonal precipitation amounts and shows the impact of scenario S1 on the surface mass balance over the transition period.

The impact of the scenarios for the year 2004-2005 highlighted the fact that the temporal distribution of the precipitation is indeed very important, but that precipitation amounts also play a key role in mass loss.

The three scenarios described here show that selecting a high precipitation threshold value had a mitigated impact on the melt rate. For years with average or above average seasonal precipitation (see Table 4), it reduced melt more than the reference run but less than scenario S1. For years with less than average seasonal precipitation, it prevented the formation of a thick snow-pack thereby yielding a higher melt rate than the reference run. Finally, grouping all the precipitation events at the beginning of the month tended to increase the melt rate at the seasonal scale.

Because scenario S1 was the scenario that allowed the largest reduction in the melt rate over the transition period, we chose to apply this scenario to all the available years (9).

#### 4.2.2 Application of scenario S1 to the nine years

Except in two years (2011-2012 and 2012-2013), scenario S1 limited mass loss at both seasonal and annual scales (see Fig. 10a, Table 4 for the numerical values

at the seasonal scale and Table C in the Appendix for the detailed impact of the scenario per month and at both seasonal and annual scales).

Considering the 9-year average, scenario S1 reduced the melt by 14% over the transition period and by 3% at the annual scale. The mass loss limitation caused by the scenario was reduced by 43% over the transition season and by 30% at the annual scale (these values should be interpreted with caution as the scenarios sometimes cause sign inversion of the surface mass balance).

The analysis of the energy balance showed that scenario S1 reduced the net shortwave energy balance by 9% (9-y average) compared to the reference runs (Fig. 10b). This effect is directly linked to the fact that spreading out the precipitation events maintained a thicker layer of snow covering the glacier (as illustrated in Fig. 9a) and hence a higher glacier-wide albedo (as illustrated in Fig. 9b). On the other hand, the scenarios left the seasonal net longwave energy balance unchanged (due to the construction of the scenarios: at the seasonal scale, the total amount of incoming and outgoing longwave radiation is defined by the measurements).

Regarding the turbulent fluxes, considering the 9-year average, the sensible heat flux was reduced by 25% and the latent heat flux was 9% less negative when the model was run with scenario S1 compared to the reference runs. These differences are linked to the different types of glacier surface: the reference runs showed more ice covering the glacier, whereas scenario S1 maintained a thicker layer of fresh snow which reduced the roughness height of the wind on the surface (z0 snow = z0 ice/10), thereby reducing the melt rate. Finally, the impact scenario S1 had on the air temperature and relative humidity was negligible on the simulated surface mass balance.

Figure 10 confirms that the main driver of mass loss is the net shortwave energy balance: both the surface mass balance and the net shortwave radiation balance react in a very similar way (Fig. 10a, b): the more scenario S1 reduces the net shortwave energy balance, the smaller the surface mass loss.

Figure 11 illustrates the impact of scenario S1 in a year when it has a negligible impact on the surface mass balance (2012-2013, Fig.11a, b) and in a year when it has a significant impact (2005-2006, see Fig.11c, d and Table 4 for the numerical values).

In 2012-2013, because the measured precipitation events were well distributed (Fig. 11a), scenario S1 had no significant impact on their distribution over time. In terms of mass loss at the monthly scale, for September and October the positive impact of the scenario was limited, whereas the fact that one (major) precipitation event that originally occurred in November was moved to October, increased the mass loss significantly. Therefore, for this year, scenario S1 did not have much of an impact on the fresh snow cover and hence on the melt rate (Fig. 11b). Once again, for this year, seasonal precipitation during the transition period (316 mm) was below average (334 mm) and consequently a negative surface mass balance was observed over the transition period.

Conversely, for the transition period of the year 2005-2006, the observed precipitation events were concentrated (Fig. 11c). In this case, spreading out the precipitation events maintained a thicker cover of fresh snow on the glacier resulting in a higher albedo thereby reducing the net shortwave energy budget and hence the melt rate (Fig. 11d and Table 4). Additionally, the fact that the seasonal precipitation amount was 517 mm i.e., significantly higher than the long-term average, contributed to a positive surface mass balance over this period.

Scenario S1 had contrasted impacts at the annual scale, for 2005-2006, scenario S1 limited mass loss more than at the scale of the transition period (see table C in the appendix), because in this situation, the snow-pack over the glacier at the end November was thick enough to guarantee limited melt in December (until the arrival of the core wet season).

On the other hand, in years when S1 had a negligible impact (e.g., 2012-2013), redistribution of the precipitation event resulted in a thinner snow-pack in December, as a result, the glacier-wide albedo decreased and the melt rate increased, resulting in aggravated annual mass loss. Overall, when scenario S1 increased the mass loss over the transition period, it increased the annual mass loss systematically (by an average of 5%). This observation highlights the combined importance of the seasonal precipitation amounts and their temporal distribution on the melt rate in the period preceding the arrival of the core wet season.

In years with a significant mass loss (2004-2005, 2009-2010 and 2016-2017), scenario S1 reduced the mass loss by an average 13% at the scale of the transition period and by 2% at the annual scale. Similarly, in years with limited mass loss (1999-2000, 2000-2001 and 2005-2006), the mass loss was reduced by an average of 109% at the scale of the transition period and 80% at the annual scale. Such marked differences between years with limited mass loss and years with significant mass loss can be explained by both precipitation amounts and by the number of events greater than or equal to 2 mm/d that occurred during the transition period. As can be seen in Table 4, years with a significant mass loss had an average of 264 mm of precipitation during the transition period in 28 events, whereas years with limited mass loss had an average of 419 mm of precipitation in 38 events.

This study has shown that the temporal distribution of the precipitation during the transition period controlled a significant proportion of the surface mass balance: considering the 9-year average, the melt rate was reduced by 14% over the transition period. At the annual scale, it was reduced by 3%; although this difference is small it does exist, as the results were compared to the reference run thereby making it possible to eliminate modeling uncertainties.

Our investigation of the energy balance components showed that the net shortwave energy budget (via an albedo feedback effect) tends to control melt. Finally, analysis of the nine years showed that the impact of any scenario is limited if the measured precipitation events are already evenly distributed over time.

**Table 4.** Summary of the precipitation amounts and number of events above 2 mm/d along with simulated surface mass balance (SMB) and melt for both the model runs (with measurements used as model inputs and with the S1 scenario) over the transition period (September to November)

| **Years** | **Precipitation Amounts (mm)** | **Reference model run #P>2mm/d** | **Scenario S1 model run SMB (m w.e.)** | **Melt (mm)** | **SMB** |
|---|---|---|---|---|---|
| 1999-2000 | 422 | 36 | -0.12 | 554 | -0.05 |
| 2000-2001 | 318 | 29 | -0.39 | 658 | -0.16 |
| 2004-2005 | 294 | 32 | -0.99 | 1217 | -1.00 |
| 2005-2006 | 517 | 48 | 0.11 | 454 | 0.22 |
| 2008-2009 | 247 | 22 | -0.73 | 908 | -0.69 |
| 2009-2010 | 365 | 30 | -0.30 | 586 | -0.23 |
| 2011-2012 | 391 | 35 | -0.33 | 762 | -0.39 |
| 2012-2013 | 316 | 26 | -0.49 | 808 | -0.50 |
| 2016-2017 | 132 | 22 | -0.96 | 1044 | -0.90 |
| | **334** | **31** | **-0.47** | **777** | **-0.41** |
| | **110** | **8** | **0.37** | **263** | **0.40** |

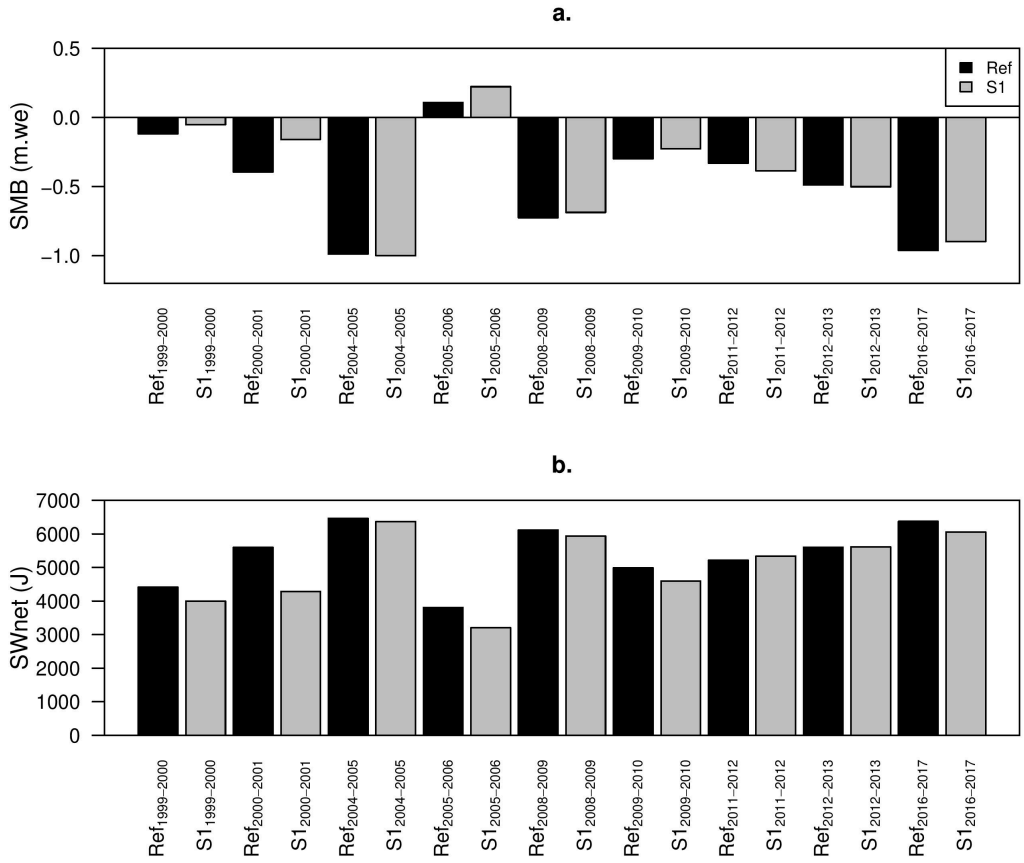


**Figur**

**10.** Plots (a) and (b) illustrate the impact of scenario S1 on the surface mass balance and on the net shortwave energy balance between September and November, respectively.

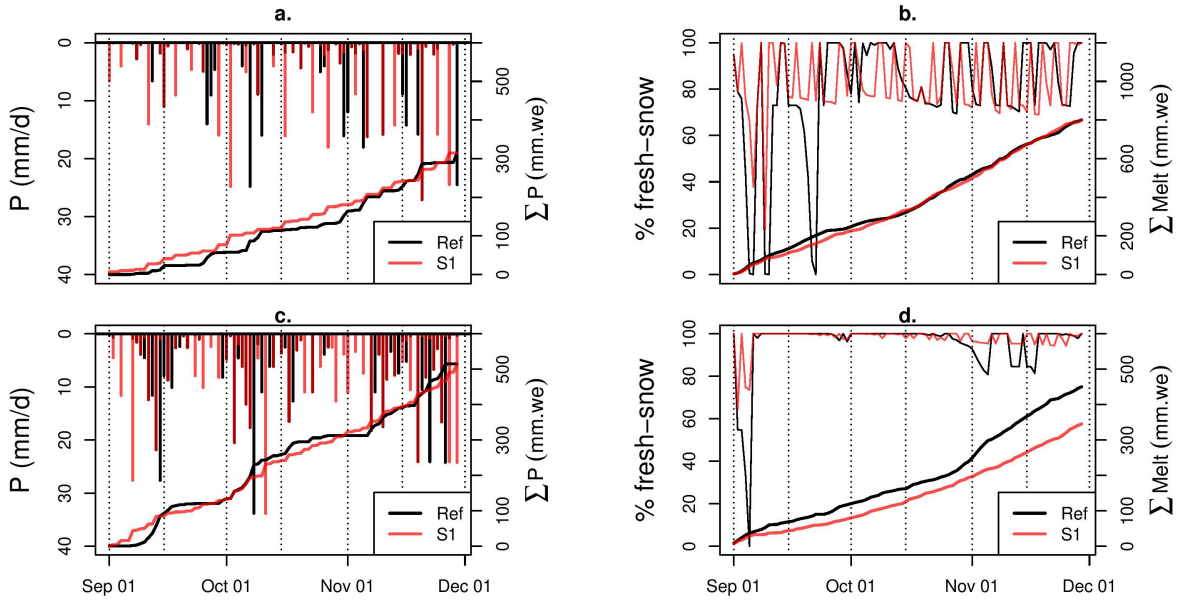


**Fi**

**11.** Plots (a) and (b) show the impact of scenario S1 on the distribution of precipitation and the percentage of fresh snow cover on the glacier (left y-axis) and melt rate (right y-axis) for a year when scenario S1 has only a limited impact on the SMB (September to November 2012). The last two plots (c and d) show the same information for the year 2005-2006 when scenario S1 significantly limits the mass loss.

4.3. Sensitivity study of the impact of cloud radiative properties on the surface mass balance

In order to assess the impact of generating long overcast conditions compared to measured conditions, the mean number of cloud events per month over 13 years was calculated based on the methodology defined in Sicart et al. (2016). Accordingly, there were 20 cloudy days in September, 25 in October, and 24 in November. Hence, on average the scenarios implied adding 10 cloudy days in September and 6 cloudy days in both October and November.

It is worth noting that the cloud radiative forcing values applied are significantly higher than the measured values: for each month, the mean cloud radiative forcing was 34% more negative than the 9-year average (as the $66^{\text{th}}$ percentile of the absolute cloud radiative forcing was used to build the scenarios). In terms of intrinsic cloud radiative properties, this increased the cloud longwave emission factor (F) by 12%, 1% and 6% in the September, October, and November scenarios, respectively. Similarly, it reduced bulk cloud shortwave transmissivity (Tn) by 33%, 14% and 9% in September, October, and November, respectively. Therefore, this scenario generation method allowed the assessment of the impact of strong sustained cloud cover on the surface mass balance.

The scenarios had a significant impact on the surface mass balance compared to the reference runs, as they systematically reduced the melt rate (the impact of the scenarios on the surface mass balance for each year is presented in Figure D in the Appendix). Considering the 9-year average, the melt rate over the transition period decreased by 6%, 15% and 20% in the September, October, and November scenarios, respectively. At the annual scale, it decreased by 2%, 5% and 6% respectively, thereby underlining the strong potential impact of clouds on the surface mass balance.

As mentioned above, the November scenario limited the mass loss most. This was true for seven out of the nine years. The two exceptions were the years 1999-2000 and 2004-2005, when the October scenario limited the melt rate most. This is because these were the only two years during which there were more clear sky days in October than in November.

Although the scenarios reduced the melt rate, which implied that the albedo in the ablation zone did not decay as fast as in the reference run because the ablation zone represents less than 20% of the surface area of the glacier, it had a limited impact on the glacier-wide albedo. In addition, the surface temperatures were not impacted by the scenarios as they were defined based on the measured outgoing longwave radiation and a -0.55 K/100 m lapse rate was applied to them.

Analysis of the turbulent fluxes showed that the hypothesis stating that the loss of physical coherence between the measured meteorological variables was negligible, was validated because over the nine years, the highest observed mean difference (considering the 9-year average) in the simulated turbulent fluxes between the scenarios and the reference runs was -5% in the October scenario.

Hence, the impact of the cloud scenarios can be assessed by looking at the incoming radiation and not the net radiation (i.e., the sum of the incoming short and longwave radiation). Considering all the years, the highest impact was for the month of November, followed by October and finally September. Figure 12 shows the surface mass balance along with the total incoming radiation during the transition period in the reference runs and in the scenarios for three years. As can be seen, the lower the incoming radiation, the lower the mass loss.

The September scenario was not the scenario with the highest impact on the surface mass balance even though it is the month with the highest average number of clear-sky days on average and the one for which the largest F and lowest Tn values were used. The limited impact can be explained by the seasonal changes in incoming radiation at the top of the atmosphere. In September, the daily mean theoretical shortwave radiation is 402 $\pm$ 13 W/m$^2$, 435 $\pm$ 6 W/m$^2$ in October, and 446 $\pm$ 1 W/m$^2$ in November. Thus, applying a cloud scenario to the month of September involved reducing less sun energy than October or November. Note that $\pm$ X W/m$^2$ represents the standard variation of the monthly theoretical amounts of incoming solar radiation at the top of the atmosphere. It is higher in September than in the other months as September is

the month when the difference in potential solar radiation between the beginning and the end of the month is highest (Fig. 3a).

To conclude, the cloud scenarios had a significant impact on the surface mass balance but these scenarios are biased and underestimated because adding overcast conditions over the whole month would most certainly add precipitation events that would further limit the mass loss. Basic statistics linking the number of cloudy days and precipitation during the transition period in the nine years showed that there is an average of one precipitation event of 4.5 mm w.e. per 1.7 cloudy days. From this information, adding 10 cloudy days in September would add six precipitation events whereas adding six cloudy days in October and November would add three to four precipitation events.

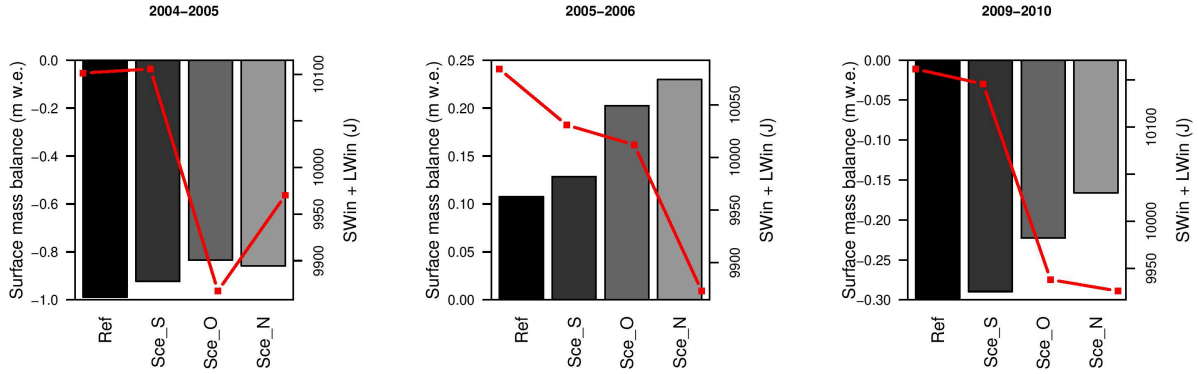


**Fi**

**12.** Impact of the three cloud scenarios on the surface mass balance over the transition period compared to the reference run (in black). The red line shows the impact of the scenarios on the incoming radiation in the three contrasted years.

## 5 Summary and conclusion

In this study, a nine-year dataset at the hourly time scale was reconstructed and used as input data for a distributed energy mass balance model on Zongo glacier. This allowed the identification of different processes that impact the melt rate and the mass balance.

To begin with, the seasons previously defined by the interannual variability of the monthly surface mass balance (e.g. Rabatel et al., 2012, 2013) or by the occurrence of precipitation and melt rates (Sicart et al., 2011) were also defined based on the cloud radiative properties: cloud radiative forcing mirrored seasonal changes and allowed the wet and dry seasons and the transition period to be defined. During the transition period, clouds have a moderate impact on the sum of the incoming short and longwave radiation with a peak distribution centered around -120 W/m$^2$. During the wet season, the clouds have a more pronounced impact on the radiative budget with a peak around -150 W/m$^2$. Such a

strong impact is typical of thick (sunlight attenuating) and warm cumulus-type clouds resulting from convective events. Finally, during the dry season, the net cloud impact on the radiative budget is low (peak around -20 $W/m^2$), which is typical of thin high-altitude clouds. The changes in cloud radiative properties have an impact on the melt rate especially during the wet season when solar attenuation is at its maximum which offsets the effect of the increased potential incoming solar radiation (as it is the austral summer).

During model calibration, we found that adjusting the digital elevation models and glacier contours for each year enhanced the simulation precision specifically for years with significant mass loss because, for these years, adjusting the size of the ablation area limits overestimation of melt.

The analysis of the 9-year mean monthly energy fluxes in the ablation zone showed that melt energy was maximum during the transition period and, to a lesser extent, during the wet season, meaning the transition season is a key period in the inter-annual variability of the surface mass balance. Although some energy was available during the dry season, most was converted into ground heat flux due to the intense night cooling of the surface of the glacier thereby shortening the daily melting period, resulting in low melt rates (as shown by Sicart et al., 2011).

The sensitivity analysis of the distribution of the precipitation events over the transition period validated the hypothesis that the frequency of precipitation events is a key driver of the interannual variability of the surface mass balance: evenly distributed precipitation events with no change in the seasonal snow amounts maintained a thicker cover of fresh snow on the surface of the glacier, which increased the glacier-wide albedo. As a result, the net shortwave radiation budget was reduced, in turn reducing the melt rate. The contrasted impacts on the melt rate reduction (very strong impact in years with average or above average seasonal precipitation amounts and less impact in years with below average precipitation) highlights the combined importance of the distribution of precipitation events over time and of the seasonal precipitation amounts.

The sensitivity analysis of the cloud distribution showed that prolonged cloudy periods in October – and more particularly in November – had the potential to dramatically reduce the melt rate at both the seasonal and annual scales. A sustained cloud cover in November had more impact than in the other months of the transition period as November is the month when potential solar irradiance is close to maximum coupled with the fact that the solar attenuation by clouds has more influence than the cloud longwave emission.

This result can be linked to the hypothesis put forward by authors who state that the arrival of the wet season plays a key role in controlling the annual surface mass balance (Francou et al., 1995, Sicart et al., 2011) in the sense that if the wet season begins in November, there will be more sustained cloudy periods which – combined with snowfall events – maintain a higher glacier wide albedo and reduce the melt rate.

All in all, the temporal distribution of precipitation is the primary driver of the interannual variability of the surface mass balance via an albedo feedback effect that reduces the net shortwave radiation budget (main driver of melt, Sicart et al., 2005) and hence the melt rate.

The next step in this study will be to apply the methodology used (to generate the scenarios for the sensitivity analysis of precipitation) to generate scenarios constrained by paleo records of temperature and precipitation (at the annual scale) to assess the climate that led to the glacier maximum extent during the Little Ice Age (between 1657±24AD and 1686±26AD, Rabatel et al., 2005, 2008). Similar studies could also be carried out on future climate using global circulation model (GCM) outputs to constrain the scenarios. Such studies would be of interest as the future of Zongo glacier is crucial both in terms of water supply and for the production of hydroelectricity.

Appendix

A – Gap filling methodology

Figure A shows the operating timelines of the three automatic weather stations on and around Zongo glacier. For the sake of simplicity, only the major data gaps (i.e.,10 days or more) are shown on the timeline. There were several overlapping operating periods (Fig. A), which made it possible to compare measurements at different stations. Thus, in order to identify the variables measured at the ORE and at the PLATAFORMA that could be used to fill in data gaps at SAMA, correlations between the variables in the same operating periods were studied and the main results are presented below. It is worth noting that, apart from the hydrological year 2016-2017, only the data measured at the ORE were required to fill in gaps in measurement made at SAMA.

It was possible to replace relative humidity data as the correlation between the measurements at the two AWS was $R^2$=0.93. Similarly, nighttime temperatures were highly correlated and could consequently be used. However, the daytime temperatures did not fit because of the different types of glacier surface (moraine and snow/ice).

Regarding the radiation components, it was possible to use both the incoming short and longwave radiation from the ORE to fill in the gaps as $R^2 > 0.8$. Regarding outgoing longwave radiation, it was found that if the values measured at the ORE above 315.6 W/m$^2$ were replaced by 315.6W/m$^2$, the measurements from the ORE could be used to replace missing values at SAMA. However, it was necessary to limit the values to 315.6W/m$^2$ for the on-glacier measurements as the surface temperature cannot exceed 0 °C.

Between May and August 2005, the incoming longwave radiation at SAMA was interrupted, consequently the incoming longwave radiation was reconstructed according to the equation parameterized by Sicart et al. (2010) at the daily time scale and was assumed to remain constant throughout the day.

Regarding precipitation, the amounts measured at the ORE and at SAMA differed significantly. The ORE was equipped with a GEONOR rain gauge located on the moraine and is consequently affected by wind, and thus showed a significant undercatch (40%) less than the amounts measured at SAMA. When gaps at SAMA were identified, two things were done, first, in order to confirm that precipitation events actually took place, the measured albedo at the AWS was analyzed as precipitation events increase the albedo value. In this case, the precipitation measured at the ORE was increased by 40% and used for to fill the gap. Because the ORE no longer existed for the hydrological year 2016-2017, the precipitation amounts measured at the PLATAFORMA were increased by 50% and used to fill in the gaps in this year. Note that the 50% increase was obtained by comparing the measured precipitation amounts on the glacier and at the PLATAFORMA over several years.

Due to the high spatial heterogeneity of wind speed in mountainous areas, the measurements made at each automatic weather station were poorly correlated. For data gaps of less than a few hours, a linear extrapolation was used. For bigger data gaps, the gap was filled with the mean values of measurements at SAMA over the same period in other years.

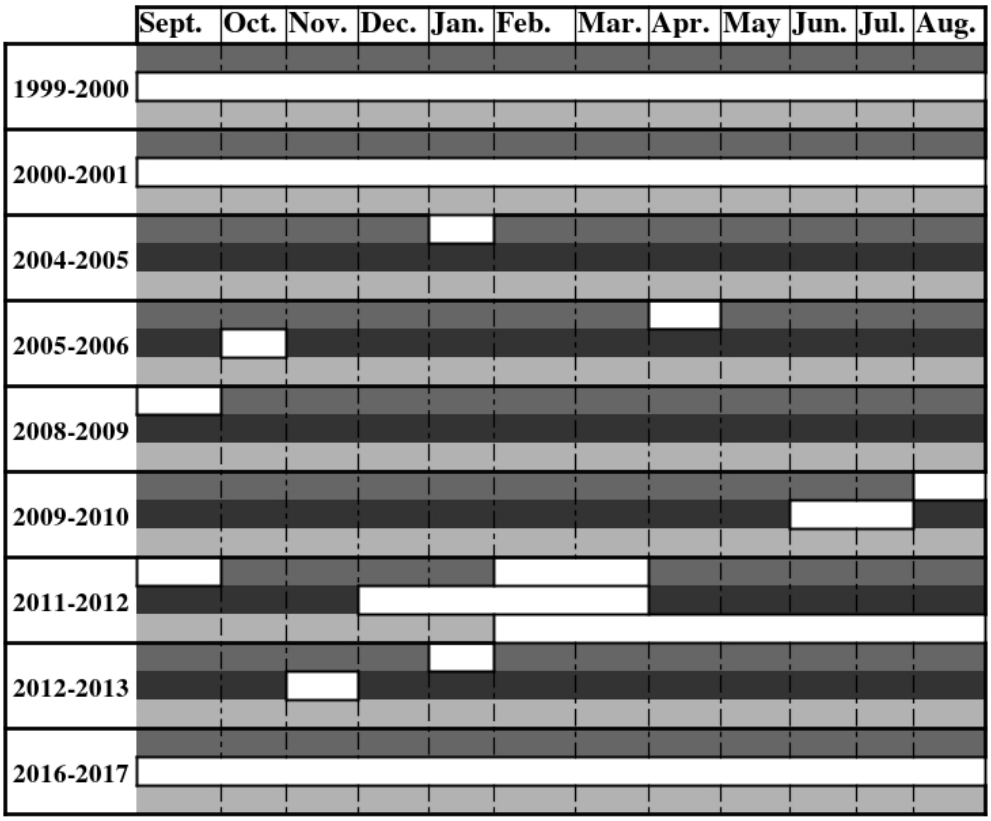


**Legend:**

| | | |
|---|---|---|
| | SAMA | Operational in all the years |
| | ORE | Operating period: 8/25/03-3/12/2015 |
| | Plataforma | Operational for all the years |
| | Represents months with data gaps > 10 days | |

**Fi**

**A.** Timeline of the operating periods of the three automatic weather stations on and around Zongo glacier. The white boxes represent months in which all the measured variables are missing for at least ten days. Note that numerous shorter periods ranging from a few hours to a few days with missing data also occurred.

B – Supplementary material for model validation

Figure B shows the specific surface mass balance according to altitude for all the modeled years. This figure highlights one of the main drawbacks of considering a single calibration for all the years: it is globally robust but, the melt in the ablation zone for some years was underestimated (e.g. 2005-2006) while for

others, it was overestimated (e.g. 2004-2005).

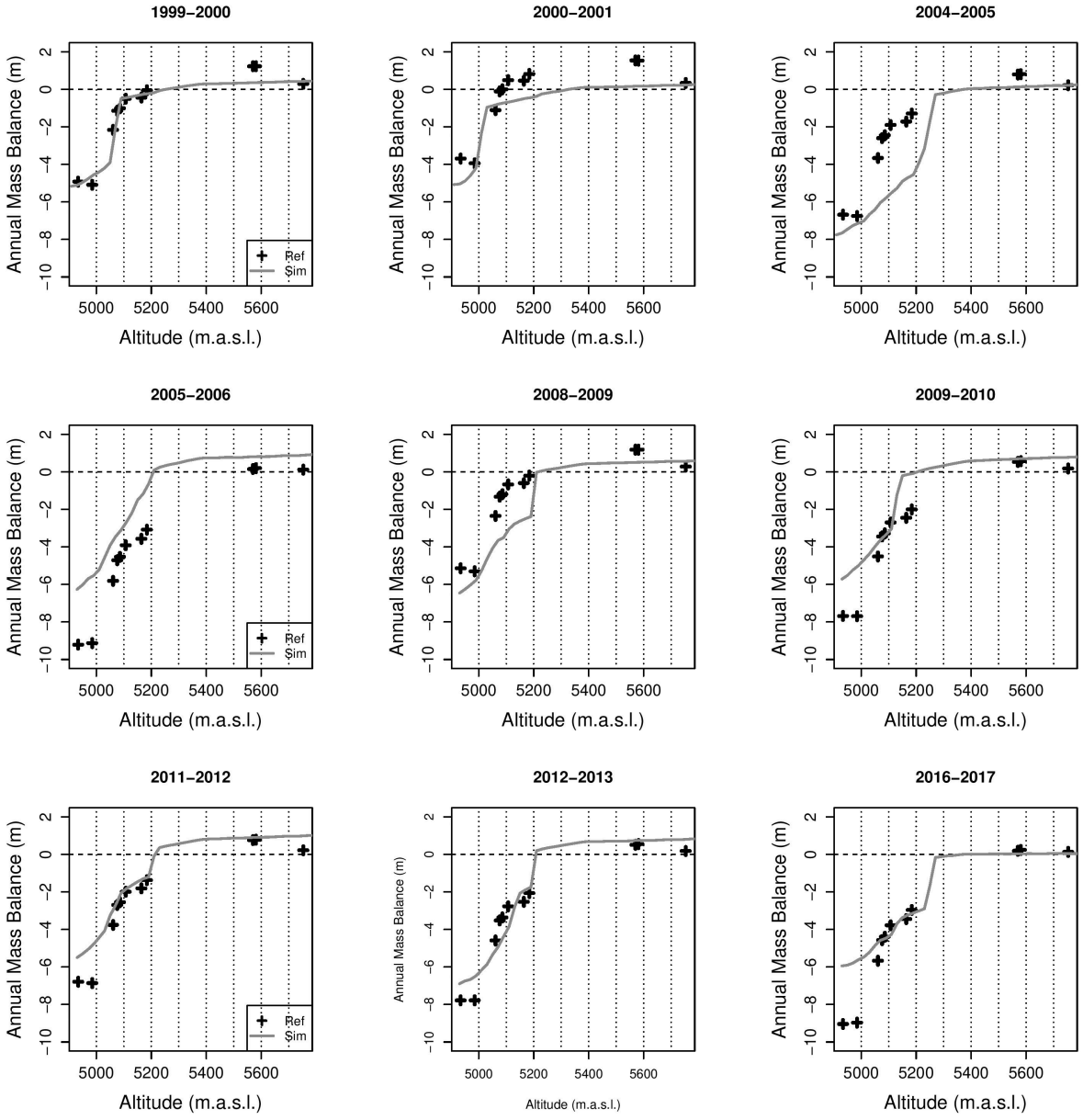


**Fi**

**B.** Specific surface mass balance according to altitude ranges. The black dots are the reference measurements. The gray lines represent the mean simulated SMB according to the altitude range (20 m elevation bands).

C – Supplementary material for precipitation sensitivity analysis

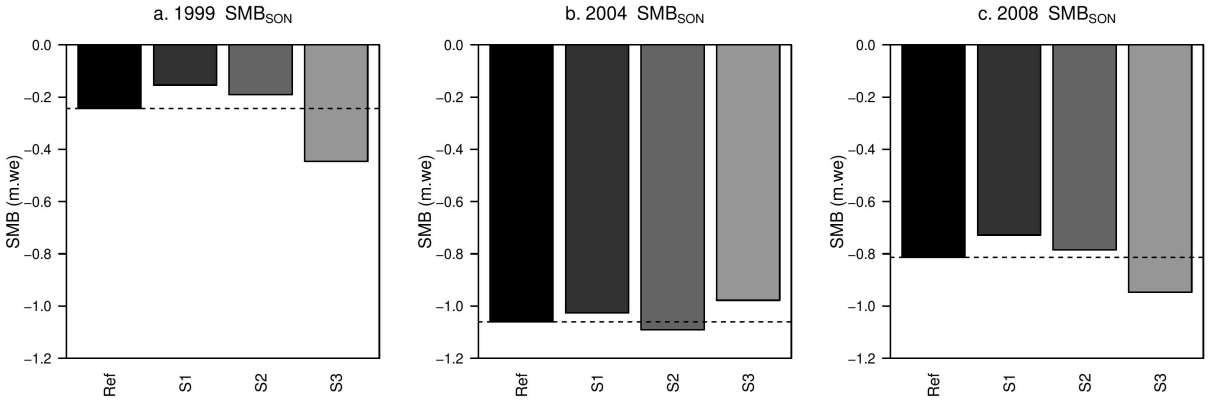


**Fig**

**C.** Impact of the S1-S3 scenarios on the surface mass balance over the transition period for the years 1999-2000 (plot a), 2004-2005 (plot b) and 2008-2009 (plot c). The dashed line shows the surface mass balance in the reference season.

**Table C.** Impact of S1 on the surface mass balance for September, October, November, the whole transition period and at the annual scale. The years in bold are those in which S1 increases the drop in surface mass-balance. The bold and italic font on the bottom right shows the mean impact on the melt at both the seasonal and annual scale.

| **Year** | **Time-scale** | **SMB ref (m w.e.)** | **SMB S1 (m w.e.)** | **Year** | **Time-scale** | **SMB ref (m w.e.)** | **SMB S1 (m w.e.)** |
|---|---|---|---|---|---|---|---|
| -2000 | September | | | -2010 | September | | |
| | October | | | | October | | |
| | November | | | | November | | |
| | S-O-N | | | | S-O-N | | |
| | Annual | | | | Annual | | |
| -2001 | September | | | **2011-2012** | **September** | **-0.03** | **-0.12** |
| | October | | | | **October** | **-0.13** | **-0.13** |
| | November | | | | **November** | **-0.17** | **-0.14** |
| | S-O-N | | | | **S-O-N** | **-0.33** | **-0.39** |
| | Annual | | | | **Annual** | **-0.89** | **-0.94** |
| -2005 | September | | | **2012-2013** | **September** | **-0.2** | **-0.17** |
| | October | | | | **October** | **-0.16** | **-0.16** |
| | November | | | | **November** | **-0.13** | **-0.17** |
| | S-O-N | | | | **S-O-N** | **-0.49** | **-0.5** |

| | | | | | |
|---|---|---|---|---|---|
| | Annual | | **Annual** | **-0.97** | **-1.01** |
| -2006 | September | -2017 | September | | |
| | October | | October | | |
| | November | | November | | |
| | S-O-N | | S-O-N | | |
| | Annual | | Annual | | |
| -2009 | September | ***Time scale*** | ***Mean difference (S1-Ref.)*** | | |
| | October | ***S-O-N*** | ***43%*** | ***55%*** | |
| | November | | | | |
| | S-O-N | ***Annual*** | ***30%*** | ***45%*** | |
| | Annual | | | | |

D – Supplementary material for cloud sensitivity analysis

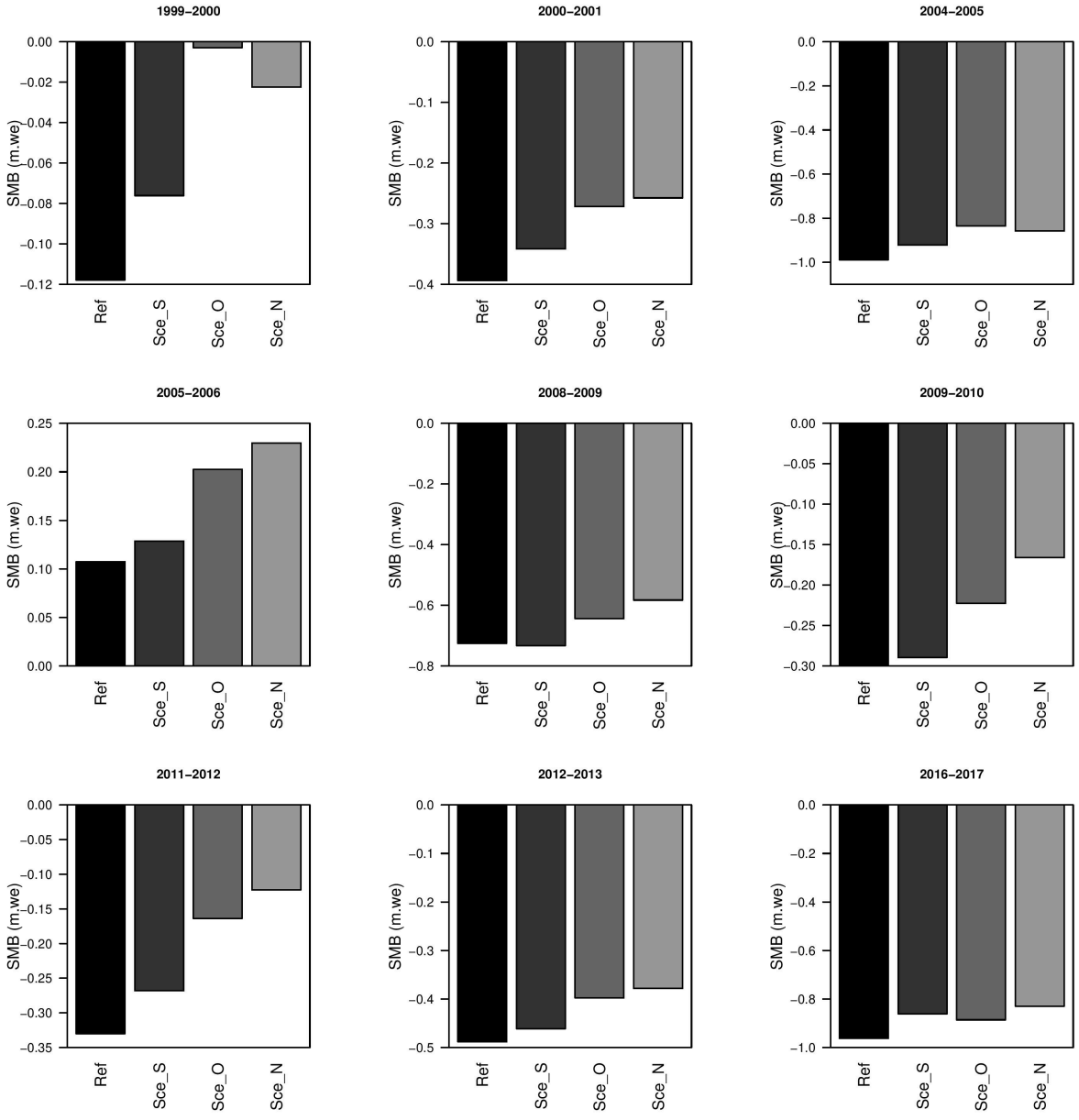


**Fi**

**D.** Impact of the cloud scenario on the surface mass balance during the transition period for the nine years considered.

References

Beljaars, A., & Holtslag, A. (1991), Flux parameterization over land surface for atmospheric models. *Journal of Applied Meteorology, 30(3),* 327–341. doi:

10.1175/1520-0450(1991)030<0327:FPOLSF>2.0.CO;2

Bradley, R. S., Keimig, F. T., Diaz, H. F., & Hardy, D. R. (2009), Recent Changes in Freezing Level Heights in the Tropics with Implications for the Deglacierization of High Mountain Regions." *Geophysical Research Letters, 36(17),* L17701. doi:10.1029/2009GL037712

Cuffey, K. M., & Paterson, W.S.B. (2010), The Physics of Glaciers. *Academic Press*. Vol. 504. Amsterdam: Cambridge University Press (CUP). doi: 10.3189/002214311796405906

Cusicanqui, D., Soruco, Á., Rabatel, A., & Anthelme, F. (2015), Mass balance of Zongo Glacier between 2006 and 2013 using volumetric method, employing Pléiades high resolution images acquired over the Cordillera Real, Bolivia (16°S, 68°W). *Revista Boliviana de Geociencias*, 8*(7),* 5–20.

Francou, B., Ribstein, P., Saravia, R., & Tiriau, E. (1995), Monthly Balance and Water Discharge of an Inter-Tropical Glacier: Zongo Glacier, Cordillera Real, Bolivia, 16°S. *Journal of Glaciology*, *41(137):,*61–67. doi:10.1017/S0022143000017767

Garreaud, R., Vuille, M., & Clement, A. C. (2003), The Climate of the Altiplano: Observed Current Conditions and Mechanisms of Past Changes. *Palaeogeography, Palaeoclimatology, Palaeoecology*, *194(1–3),* 5–22. doi: 10.1016/S0031-0182(03)00269-4

Garreaud, R. D. (2000), Intraseasonal variability of moisture and rainfall over South American Altiplano, *Monthly Weather Revue*, *128(9)*, 3337–3346, doi:10.1175/1520-0493(2000)128<3337:IVOMAR>2.0.CO;2.

Hock, R. (1998), Modelling of Glacier Melt and Discharge (Doctoral dissertation). Retrieved from: http://www.agu.org/pubs/crossref/2009/2009JD011949.shtml. Federal Institute of Technology, Switzerland.

Hock, R., & Holmgren, B. (2005), A Distributed Surface Energy-Balance Model for Complex Topography and Its Applications to Storglaciaren. *Journal of Glaciology, 51(172),* 25–36. doi: 10.3189/172756505781829566

Hock, R., & Tijm-Reijmer, C. (2012), A Mass-Balance, Glacier Runoff and Multi-Layer Snow Model DEBAM and DETIM Distributed Energy Balance and Distributed Enhanced Temperature Index Model Users Manual. http://www2.gi.alaska.edu/~regine/modelmanual.pdf.

Kaser, G. (1999), A Review of the Modern Fluctuations of Tropical Glaciers. *Global and Planetary Change,* 22*(1–4)*, 93–103. doi: 10.1016/S0921-8181(99)00028-4

Kaser, G. (2001), Glacier-Climate Interaction at Low Latitudes. *Journal of Glaciology, 47(157)*, 195–204. doi: 10.3189/172756501781832296

Kaser, G., Ames, A., & Zamora, M. (1990), Glacier Fluctuations and Climate in the Cordillera Blanca, Peru." *Annals of Glaciology, 14(May),* 136–40. doi:

10.1017/s0260305500008430

Lejeune, Y., Wagnon, P., Bouilloud, L., Chevallier, P., Etchevers, P., Martin, E., Sicart, J.E., & Habets, F. (2007), Melting of Snow Cover in a Tropical Mountain Environment in Bolivia: Processes and Modeling. *Journal of Hydrometeorology, 8(4),* 922-37. doi: 10.1175/JHM590.1.

Lenters, J. D., & Cook, K. H. (1997), On the Origin of the Bolivian High and Related Circulation Features of the South American Climate. *Journal of the Atmospheric Sciences, 54(5),* 656–77. doi: 10.1175/1520-0469(1997)054

Litt, M., Sicart, J. E., Helgason, W. D., & Wagnon, P. (2014), Turbulence Characteristics in the Atmospheric Surface Layer for Different Wind Regimes over the Tropical Zongo Glacier (Bolivia, 16 S)." *Boundary-Layer Meteorology, 154(3),* 471–95. doi: 10.1007/s10546-014-9975-6.

Masiokas, M. H., Rabatel, A., Rivera, A., Ruiz, L., Pitte, P., Ceballos, J.L., Barcaza, G., Soruco, A., Brown, F., Dussaillant, I., & MacDonell, S. (2020), A Review of the Current State and Recent Changes of the Andean Cryosphere. *Frontiers in Earth Science, 8 (June),* 1–27. doi: 10.3389/feart.2020.00099.

Maussion, F., Gurgiser, W., Großhauser, M., Kaser, G., and Marzeion, B. (2015), ENSO influence on surface energy and mass balance at Shallap Glacier, Cordillera Blanca, Peru, *The Cryosphere, 9(4),* 1663–1683. doi: 10.5194/tc-9-1663-2015, 2015.

Mölg, T., Cullen, N. J., Hardy, D. R., Kaser, G., & Klok, L. (2008), Mass Balance of a Slope Glacier on Kilimanjaro and Its Sensitivity to Climate Thomas. *International Journal of Climatology, 28(6),* 881–92. doi: 10.1002/joc.1589

Mölg, T., Cullen, N. J.,& Kaser, G. (2009), Solar Radiation, Cloudiness and Longwave Radiation over Low-Latitude Glaciers : Implications for Mass-Balance Modeling. *Journal of Glaciology, 55(190),* 292–302. doi: 10.3189/002214309788608822

Nicholson, L. I., Prinz, R., Mölg, T., & G. Kaser, G. (2013), Micrometeorological Conditions and Surface Mass and Energy Fluxes on Lewis Glacier, Mt Kenya, in Relation to Other Tropical Glaciers. *Cryosphere, 7(4),* 1205–25. doi: 10.5194/tc-7-1205-2013

Oerlemans, J., & Knap, W. H. (1998), A 1 Year Record of Global Radiation and Albedo in the Ablation Zone of Morteratschgletscher, Switzerland. *Journal of Glaciology, 44 (147),* 231–38. doi: 10.3189/s0022143000002574

Østby, T. I., Schuler, T. V., Hagen, J. O., Hock, R., Kohler, J., & Reijmer C.H. (2017), Diagnosing the Decline in Climatic Mass Balance of Glaciers in Svalbard over 1957-2014. *Cryosphere, 11(1),* 191–215. doi: 10.5194/tc-11-191-2017

Paulson, C.A. (1970), The mathematical representation of wind speed and temperature profiles in the unstable atmospheric surface layer. *Journal of Applied Meteorology, 9,* 857-861. doi: 10.1175/1520-0450(1970)009<0857:TMROWS>2.0.CO;2

Prinz, R., Nicholson, L. I., Mölg, T., Gurgiser, W., & Kaser, G. (2016), Climatic Controls and Climate Proxy Potential of Lewis Glacier, Mt. Kenya. *Cryosphere, 10(1),* 133–48. doi: 10.5194/tc-10-133-2016

Rabatel, A., Bermejo, A., Loarte, E., Soruco, A., Gomez, J., Leonardini, G., Vincent, C., & Sicart, J.E. (2012), Can the Snowline Be Used as an Indicator of the Equilibrium Line and Mass Balance for Glaciers in the Outer Tropics? *Journal of Glaciology, 58(212)*, 1027–36. doi: 10.3189/2012JoG12J027

Rabatel, A., Jomelli, V., Francou, B., Naveau, P., & Grancher, D. (2008), The Little Ice Age in the tropical Andes of Bolivia (16°S) and its implication for a climate reconstruction. *Quaternary Research*, *70(2),* 198-212. doi: 10.1016/j.yqres.2008.02.012

Rabatel, A., Francou, B., Soruco, A., Gomez, J., Cáceres, B., Ceballos, J. L., Basantes, R., et al. (2013), Current State of Glaciers in the Tropical Andes: A Multi-Century Perspective on Glacier Evolution and Climate Change. *Cryosphere, 7(1),* 81–102. doi: 10.5194/tc-7-81-2013

Rabatel, A., Jomelli, V., Naveau, P., Francou, B., & Grancher, D. (2005), Dating fluctuations of glaciers during the Little Ice Age in the tropical Andes: Charquini glaciers (Bolivia, 16°S). *Comptes-Rendus Géoscience, 337(15),* 1311-1322. doi:0.1016/j.crte.2005.07.009.

Ramallo, C (2013), Caractérisation du régime pluviométrique et sa relation à la fonte du Glacier Zongo (Cordillère Royale) (Doctoral dissertation). Retrieved from: https://tel.archives-ouvertes.fr/tel-01548283. Université Grenoble Alpes.

Reijmer, C. H., & Hock, R. (2008), Internal Accumulation on Storglaciären, Sweden, in a Multi-Layer Snow Model Coupled to a Distributed Energy- and Mass-Balance Model. *Journal of Glaciology, 54(184),* 61–72. doi: 10.3189/002214308784409161

Réveillet, M., Rabatel, A., Gillet-Chaulet, F., & Soruco, A. (2015), Simulations of Changes to Glaciar Zongo, Bolivia (16° S), over the 21st Century Using a 3-D Full-Stokes Model and CMIP5 Climate Projections. *Annals of Glaciology, 56 (70),* 89–97. doi: 10.3189/2015AoG70A113

Ribstein, P., Tiriau, E., Francou, B., & Saravia, R. (1995), Tropical Climate and Glacier Hydrology: A Case Study in Bolivia. *Journal of Hydrology, 165(1–4),* 221–34. doi: 10.1016/0022-1694(94)02572-S

Sicart, J. E. (2002), Contribution à l'étude Des Flux d'énergie, Du Bilan de Masse et Du Débit de Fonte d'un Glacier Tropical: Le Zongo, Bolivie (Doctoral dissertation). Retrieved from http://hydrologie.org/THE/SICART.pdf. Université Paris IV Pierre et Marie Curie.

Sicart, J. E., Espinoza, J. C., Quéno, L., & Medina, M. (2016), Radiative Properties of Clouds over a Tropical Bolivian Glacier: Seasonal Variations and Relationship with Regional Atmospheric Circulation. *International Journal of Climatology, 36(8),* 3116–28. doi: 10.1002/joc.4540

Sicart, J.E, Hock, R., & Six, D. (2008), Glacier Melt, Air Temperature, and Energy Balance in Different Climates: The Bolivian Tropics, the French Alps, and Northern Sweden. *Journal of Geophysical Research Atmospheres, 113(24),* 1–11. doi: 10.1029/2008JD010406

Sicart, J. E., Hock, R., Ribstein, P., & Chazarin, J. P. (2010), Sky Longwave Radiation on Tropical Andean Glaciers: Parameterization and Sensitivity to Atmospheric Variables. *Journal of Glaciology, 56(199),* 854–60. doi: 10.3189/002214310794457182

Sicart, J. E., Hock, R., Ribstein, P., Litt, M., & Ramirez, E. (2011), Analysis of Seasonal Variations in Mass Balance and Meltwater Discharge of the Tropical Zongo Glacier by Application of a Distributed Energy Balance Model. *Journal of Geophysical Research, 119(D13),* 1–18. doi: 10.1029/2010JD015105

Sicart, J. E., Ribstein, P., Chazarin, J. P., & Berthier, E. (2002), Solid precipitation on a tropical glacier in Bolivia measured with an ultrasonic depth gauge." *Water Resources Research*, *38(10),* 7–1–7–7.

doi: 10.1029/2002WR001402

Sicart, J. E., Wagnon, P., & Ribstein, P. (2005) Atmospheric Controls of the Heat Balance of Zongo Glacier (16°S, Bolivia). *Journal of Geophysical Research Atmospheres, 110(12),* 1–17. doi: 10.1029/2004JD005732

Soruco, A., Vincent, C., Francou, B., Ribstein, P., Berger, T., Sicart, J. E., Wagnon, P., Arnaud, Y., Favier, V., & Lejeune, I. (2009), Mass Balance of Glaciar Zongo, Bolivia, between 1956 and 2006, Using Glaciological, Hydrological and Geodetic Methods. *Annals of Glaciology, 50(50),* 1–8. doi: 10.1039/C39920000859

Soruco, A., Vincent, C., Rabatel, A., Francou, B., Thibert, E., Sicart, J. E., & Condom, T. (2015), Contribution of Glacier Runoff to Water Resources of La Paz City, Bolivia (16° S). *Annals of Glaciology, 56(70),* 147–54. doi: 10.3189/2015AoG70A001

Troll, C. (1941), Studien zur vergleichenden Geographie der Hochgebirge der Erde. Bonner Mitt. 21, Universität Bonn, Bonn, Germany.

Vincent, C., Soruco, A., Azam, M. F., Basantes-Serrano, R., Jackson, M., Kjøllmoen, B., Thibert, E., et al. (2018), A Nonlinear Statistical Model for Extracting a Climatic Signal From Glacier Mass Balance Measurements. *Journal of Geophysical Research: Earth Surface, 123(9),* 2228–42. doi: 10.1029/2018JF004702

Vuille, M., Hardy, D. R., Braun, C., Keimig, F., & Bradley, R. S. (1998), Atmospheric Circulation Anomalies Associated with 1996/1997 Summer Precipitation Events on Sajama Ice Cap, Bolivia. *Journal of Geophysical Research, 103(D10),* 191–204. doi: 10.1029/98jd00681

Wagnon, P., Ribstein, P., Francou, B., & Pouyaud, B. (1999), Annual Cycle of

Energy Balance of Zongo Glacier, Cordillera Real, Bolivia. *Journal of Geophysical Research, 104 (D4),* 3907–23. doi: 10.1029/1998JD200011